Supporting information for

Unleashing the Potential of 1,3-Diketone Analogs as Selective LH2 Inhibitors

Juhoon Lee,[1] Hou-fu Guo,[2] Shike Wang,[3] Yazdan Maghsoud,[4] Erik Antonio Vázquez-Montelongo,[5] Zhifeng Jing,[6] Rae M Sammons,[1] Eun Jeong Cho,[1] Pengyu Ren,[6] G. Andrés Cisneros,[4,7] Jonathan M. Kurie,[3] and Kevin N. Dalby,[*,1]

[1]*Division of Chemical Biology and Medicinal Chemistry, College of Pharmacy, University of Texas at Austin, Austin, Texas 78712, USA; Targeted Therapeutic Drug Discovery and Development Program, College of Pharmacy, University of Texas, Austin, TX 78712, USA*
**E-mail: dalby@austin.utexas.edu*
[2]*Department of Molecular and Cellular Biochemistry, University of Kentucky College of Medicine, KY 40536, USA*
[3]*Departmnt of Thoracic/Head and Neck Medical Oncology, The University of Texas MD Anderson Cancer Center, Houston, TX 77030, USA*
[4]*Department of Chemistry and Biochemistry, The University of Texas at Dallas, Richardson, TX 75080, USA*
[5]*Department of Physical Medicine and Rehabilitation, The University of Texas Southwestern Medical Center, Dallas, TX 75390, USA*
[6]*Department of Biomedical Engineering, The University of Texas at Austin, Austin, TX 78712, USA*
[7]*Department of Physics, The University of Texas at Dallas, Richardson, TX 75080, USA*

Table of contents

1. Experimental section

§ *No unexpected or unusually high safety hazards were encountered*

1-1. Chemistry

All chemical reagents and solvents were purchased from commercial sources, including Aldrich, TCI, and Acros, and were used without additional purification. **1** and **2** were purchased from Oakwood Chemical. NMR spectra were recorded on Agilent MR 400 MHz and Bruker AVIII 500 MHz instruments. The NMR spectra were referenced to solvent, and the spectroscopic solvents were purchased from Cambridge Isotope Laboratories. Chemical ionization (CI) and electrospray ionization (ESI) mass spectra were recorded on a VG ZAB-2E instrument and a VG AutoSpec apparatus. TLC analyses used Sorbent Technologies silica gel (200 mm) sheets. Column chromatography was performed on Sorbent silica gel 60A (40–63 mm) or neutral alumina (50–200 mm, Brockmann grade II).

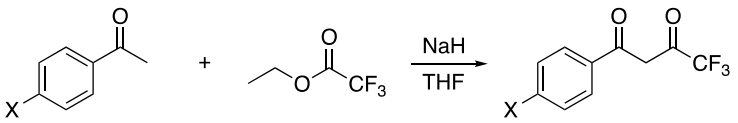

1a X = F
1b X = NO_2

2a

3 X = F
4 X = NO_2

*General procedure for the syntheses of **3** and **4** (**4** as an example)*: To a solution of 4'-nitroacetophenone (330 mg, 2 mmol) in 2 mL of tetrahydrofuran (THF), sodium hydride (60% dispersion in mineral oil) (88 mg, 2.2 mmol) was added at 0 °C under stirring. The mixture was stirred for 30 minutes, followed by the dropwise addition of ethyl trifluoroacetate (0.262 mL, 2.2 mmol) at room temperature. The reaction mixture was stirred for an additional 12 hours at room

temperature. The reaction was then concentrated and diluted with ethyl acetate, washed with 1N hydrochloric acid and brine, and dried over Na_2SO_4. The crude product was purified by column chromatography on silica gel (using an ethyl acetate/hexane eluent in a 1:2 ratio) to obtain a yellow oil. The product was recrystallized from an ethyl acetate/dichloromethane/hexane mixture to afford the final compound.

4,4,4-trifluoro-1-(4-fluorophenyl)butane-1,3-dione (***3***) : White solid; Yield: 85% ^{1}H NMR (400MHz, DMSO-d6): δ 8.23-8.19 (d, 2H, Ar*H*), 7.43-7.39 (d, 2H, Ar*H*), 7.00 (s, 1H, C=C*H*). ^{13}C NMR (100 MHz, DMSO-d_6): δ 185.1, 173.5, 173.1, 167.1, 164.6, 131.3, 129.4, 129.3, 118.7, 116.4, 116.2, 93.2. HRMS (ESI) *m/z* 235.0382 calcd for $C_{10}H_7F_4O_2$, found 235.0382.

*4,4,4-trifluoro-1-(4-nitrophenyl)butane-1,3-dione (**4**)* : Yellow solid; Yield: 75% ^{1}H NMR (500MHz, DMSO-d_6): δ 8.29-8.27 (d, 2H, Ar*H*), 8.13-8.11 (d, 2H, Ar*H*), 6.38 (s, 1H, C=C*H*). ^{13}C NMR (125 MHz, DMSO-d_6): δ 185.8, 172.3, 172.1, 171.9, 149.3, 144.0, 128.6, 123.8, 122.1, 120.0, 117.6, 115.3, 90.5. HRMS (M_{mi}) *m/z* 261.0249 (M+) calcd for $C_{10}H_6F_3NO_4$, found 261.0248

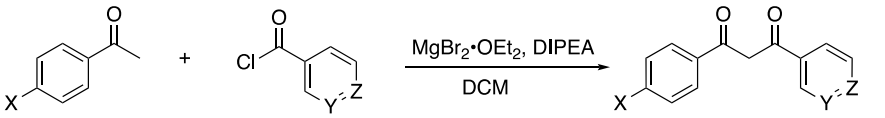

*General procedure for the syntheses of **5–8** (**5** as an example)*: A solution of acetophenone (0.117 mL, 1 mmol) and nicotinyl chloride hydrochloride (196 mg, 1.1 mmol) in dichloromethane

(5 mL) was prepared. To this solution, magnesium bromide ethyl etherate (697.2 mg, 2.7 mmol) was added, and the resulting mixture was stirred at room temperature for 15 minutes. Next, N,N-Diisopropylethylamine (0.82 mL, 4.7 mmol) was added dropwise to the mixture using a syringe over 1 minute, and the reaction was stirred at room temperature for 12 hours. The resulting crude product was diluted with a mixture of H_2O and methanol, and 1N HCl was added to the mixture until a pH of 4-5 was achieved. The aqueous crude was then extracted with dichloromethane, and the organic phase was dried over Na_2SO_4. The crude product was purified by column chromatography over silica gel, using an eluent mixture of ethyl acetate and hexane in a 1:3 ratio. The resulting product was obtained as a yellow solid.

1-phenyl-3-(pyridin-3-yl)propane-1,3-dione (**5**): Yellow solid, Yield: 29% ^{1}H NMR (500MHz, $CDCl_3$): δ 16.65 (s, 1H, O*H*), 9.23 (s, 1H, Py*H*), 8.80-8.79 (d, 1H, Py*H*), 8.39-8.37(d, 1H, Py*H*), 8.02-8.00 (d, 2H, Ar*H*), 7.60-7.58 (m, 1H, Ar*H*), 7.53-7.52 (m, 3H, Ar*H,* Py*H*), 6.88 (s, 1H, C=C*H*). ^{13}C NMR (125MHz, $CDCl_3$): δ 186.7, 182.5, 151.3, 147.2, 135.8, 134.9, 133.1, 131.9, 128.9, 127.4, 124.1, 93.6. HRMS (ESI) *m/z* 226.0863 $(M+H)^+$ calcd for $C_{14}H_{11}NO_2$, found 226.0865.

1-phenyl-3-(pyridin-4-yl)propane-1,3-dione (**6**): Yellow solid, Yield: 22% ^{1}H NMR (400MHz, $CDCl_3$): δ 16.49 (s, 1H, O*H*), 8.82-8.80 (d, 2H, Py*H*), 8.02-8.00 (d, 2H, Ar*H*), 7.83-7.81(d, 2H, Py*H*), 7.62-7.58 (m, 1H, Ar*H*), 7.54-7.50 (m, 2H, Ar*H*), 6.89 (s, 1H, C=C*H*). ^{13}C NMR (100MHz, $CDCl_3$): δ 188.5, 180.9, 150.1, 142.8, 135.2, 133.2, 128.8, 127.5, 120.6, 94.1. HRMS (ESI) *m/z* 226.0863 $(M+H)^+$ calcd for $C_{14}H_{11}NO_2$, found 226.0863.

1-(pyridin-3-yl)-3-(4-(trifluoromethyl)phenyl)propane-1,3-dione (**7**): Yellow solid, Yield: 20% ^{1}H NMR (400MHz, $CDCl_3$): δ 16.44 (s, 1H, O*H*), 9.24 (s, 1H, Py*H*), 8.80 (d, 1H, Py*H*), 8.34-8.32 (d, 1H, Py*H*), 8.11-8.09 (d, 2H, Ar*H*), 7.78-7.76 (d, 2H, Ar*H*), 7.52-7.49 (m, 1H, Py*H*), 6.89 (s, 1H, C=C*H*). ^{13}C NMR (100MHz, $CDCl_3$): δ 184.3, 184.2, 152.5, 148.0, 138.1, 134.3, 134.0, 131.2, 127.6, 125.8, 124.9, 123.9, 122.2, 94.0. ^{19}F NMR (376 MHz, $CDCl_3$) δ -63.10. HRMS (ESI) *m/z* 294.0736 $(M+H)^+$ calcd for $C_{15}H_{10}F_3NO_2$, found 294.0741.

1-(4-nitrophenyl)-3-(pyridin-3-yl)propane-1,3-dione (**8**): Yellow solid, Yield: 15% ^{1}H NMR (500MHz, DMSO-d_6): δ 9.40 (s, 1H, Py*H*), 8.85 (d, 1H, Py*H*), 8.57-8.55 (d, 1H, Py*H*), 8.44-8.38 (d, 4H, Ar*H*), 7.68-7.59 (d, 1H, Py*H*), 7.59 (s, 1H, C=C*H*). ^{13}C NMR (125MHz, DMSO-d_6): δ 186.1, 182.1, 153.7, 150.4, 149.1, 140.1, 136.0, 130.8, 129.3, 124.6, 124.4, 95.9. HRMS (ESI) *m/z* 271.0713 $(M+H)^+$ calcd for $C_{14}H_{10}N_2O_4$, found 271.0716.

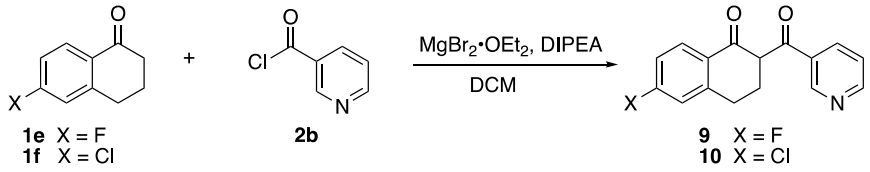

*General procedure for the syntheses of **9** and **10** (**9** as an example)*: A solution of 6-fluoro-1-teralone (164.2 mg, 1 mmol) and nicotinyl chloride hydrochloride (196 mg, 1.1 mmol) in dichloromethane (5 mL) was prepared. To this solution, magnesium bromide ethyl etherate (697.2 mg, 2.7 mmol) was added, and the resulting mixture was stirred at room temperature for 15 minutes. Next, N,N-Diisopropylethylamine (0.82 mL, 4.7 mmol) was added dropwise to the mixture using a syringe over 1 minute, and the reaction was stirred at room temperature for 12 hours. The resulting crude product was diluted with a mixture of H_2O and methanol, and 1N HCl was added

to the mixture until a pH of 4-5 was achieved. The aqueous crude was then extracted with dichloromethane, and the organic phase was dried over Na_2SO_4. The crude product was purified by column chromatography over silica gel, using an eluent mixture of ethyl acetate and hexane in a 1:3 ratio. The resulting product was obtained as a yellow solid.

6-fluoro-2-nicotinoyl-3,4-dihydronaphthalen-1(2H)-one (**9**): Yellow solid, Yield: 23% ^{1}H NMR (400MHz, $CDCl_3$): δ 16.77 (s, 1H, O*H*), 8.85 (s, 1H, Py*H*), 8.74-8.73 (d, 1H, Py*H*), 8.08-8.05 (m, 2H, Py*H*), 7.56-7.53 (d, 1H, Ar*H*), 7.08-7.04 (t, 1H, Ar*H*), 6.95-6.92 (d, 1H, Ar*H*), 2.87-2.76 (m, 4H, CH_2). ^{19}F NMR (376 MHz, $CDCl_3$) δ -104.57. HRMS (ESI) *m/z* 270.0925 $(M+H)^+$ calcd for $C_{16}H_{12}FNO_2$, found 270.0932.

6-chloro-2-nicotinoyl-3,4-dihydronaphthalen-1(2H)-one (**10**): Yellow solid, Yield: 56% ^{1}H NMR (400MHz, $CDCl_3$): δ 16.63 (s, 1H, O*H*), 8.85 (s, 1H, Py*H*), 8.74-8.73 (d, 1H, Py*H*), 8.03-8.01 (d, 1H, Py*H*), 7.98-7.96 (d, 1H, Py*H*) 7.53-7.50 (t, 1H, Ar*H*), 7.37-7.34 (d, 1H, Ar*H*), 7.25-7.24 (s, 1H, Ar*H*), 2.84-2.77 (m, 4H, CH_2). ^{13}C NMR (100MHz, $CDCl_3$): δ 184.0, 180.7, 150.0, 147.6, 143.1, 139.2, 136.8, 130.2, 128.2, 127.8, 127.5, 123.8, 106.5, 28.4, 24.4. HRMS (ESI) *m/z* 286.0629 $(M+H)^+$ calcd for $C_{16}H_{12}ClNO_2$, found 286.0634.

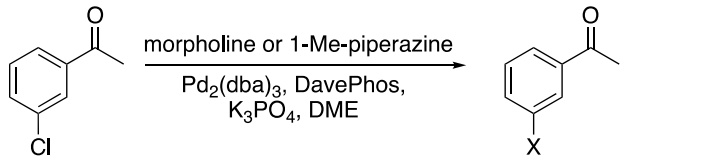

3-Chloroacetophenone

1g X = morpholine
1h X = 1-Me-piperazine

*General procedure for synthesizing **1g** and **1h** (**1h** as an example)*: a two-neck round bottom flask was first evacuated and backfilled with argon. $Pd_2(dba)_3$ (82.4 mg, 0.09 mmol), DavePhos (70.84 mg, 0.18 mmol), and K_3PO_4 (891.5 mg, 4.2 mmol) were then added to the flask. The flask was again evacuated and backfilled with argon before being capped with a rubber septum. Next, 3-chloroacetophenone (0.4 mL, 3.0 mmol) and 1-methylpiperazine (0.4 mL, 3.6 mmol) were added to the flask via syringe through the septum. The resulting mixture was stirred at 100°C under argon for 12 hours. After completion of the reaction, the solution was cooled to room temperature and diluted with diethyl ether. The mixture was then filtered through Celite to remove any impurities. The resulting crude product was purified by silica gel column chromatography using dichloromethane:methanol (40:1) as the eluent to obtain brown liquid.

1-(3-morpholinophenyl)ethan-1-one (**1g**): Brown solid, Yield: 63% ^{1}H NMR (400MHz, $CDCl_3$): δ 7.48-7.47 (s, 1H, Ar*H*), 7.42-7.40 (d, 1H, Ar*H*), 7.35-7.31 (t, 1H, Ar*H*), 7.10-7.07 (d, 1H, Ar*H*) 3.85-3.82 (m, 4H, CH_2), 3.19-3.16 (m, 4H, CH_2), 2.56 (s, 3H, C=O-CH_3). ^{13}C NMR (100MHz, $CDCl_3$): δ 198.3, 151.4, 138.0, 129.3, 120.3, 114.4, 66.7, 49.0, 26.7. HRMS (ESI) *m/z* 206.1176 $(M+H)^+$ calcd for $C_{12}H_{15}NO_2$, found 206.1177.

1-(3-(4-methylpiperazin-1-yl)phenyl)ethan-1-one (**1h**): Brown liquid, Yield: 74% ^{1}H NMR (400MHz, $CDCl_3$): δ 7.51-7.50 (s, 1H, Ar*H*), 7.43-7.41 (d, 1H, Ar*H*), 7.36-7.32 (t, 1H, Ar*H*), 7.13-7.11 (d, 1H, Ar*H*) 3.32-3.29 (m, 4H, CH_2), 2.66-2.64 (m, 4H, CH_2), 2.58 (s, 3H, C=O-CH_3), 2.40 (s, 3H, N-CH_3). ^{13}C NMR (100MHz, $CDCl_3$): δ 198.5, 151.2, 138.0, 129.3, 120.6, 120.1,

114.9, 54.8, 48.6, 45.9, 26.8. HRMS (ESI) *m/z* 219.1492 $(M+H)^+$ calcd for $C_{13}H_{18}N_2O$, found 219.1498.

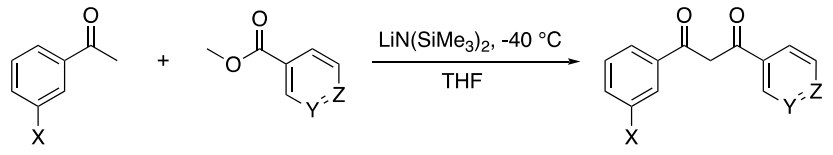

1g X = morpholine
1h X = 1-Me-piperazine

2d Y = N, Z = CH
2e Y = CH, Z = N
2f Y = CH, Z = CCH_3

11 X = morpholine, Y = N, Z= CH
12 X = morpholine, Y = CH, Z = N
13 X = 1-Me-piperazine, Y = CH, Z = N
18 X = morpholine, Y = CH, Z = CCH_3

*General procedure for the syntheses of **11–13** and **18** (**12** as an example)*: A solution of 1-(3-morpholinophenyl)ethan-1-one (**1g**) (102.6 mg, 0.5 mmol) was placed in an 8 mL vial and evacuated and backfilled with argon. Next, 2 mL of THF was added to the vial, and the solution was cooled to -40 ºC. A solution of lithium bis(trimethylsilyl)amide ($LiN(SiMe_3)_2$) in THF (1.0 M, 1.1 mL, 1.1 mmol) was then added dropwise to the reaction mixture over 20 minutes. The reaction mixture was stirred at -40 ºC for 10 minutes. And then, a solution of methyl isonicotinate (75.4 mg, 0.55 mmol) in THF (2 mL) was added dropwise to the reaction mixture and stirred at room temperature for 6 hours. The resulting orange solution was then dried *in vaccuo*, and the crude product was purified by silica gel column chromatography using an eluent of ethylacetate:hexanes (1:5) to afford the compound.

*1-(3-morpholinophenyl)-3-(pyridin-3-yl)propane-1,3-dione (**11**)*: Brown solid, Yield: 60%, ^{1}H NMR (500MHz, $CDCl_3$): δ 16.67 (s, 1H, O*H*), 9.24 (s, 1H, Py*H*), 8.78 (s, 1H, Py*H*), 8.38-8.36 (d, 1H, Py*H*), 7.58 (s, 1H, Ar*H*), 7.58-7.52 (t, 1H, Py*H*), 7.49-7.47 (d, 1H, Ar*H*), 7.42-7.38 (t, 1H, Ar*H*), 7.19-7.16 (d, 1H, Ar*H*), 6.86 (s, 1H, C=C*H*), 3.92-3.89 (m, 4H, CH_2), 3.27-3.25 (m, 4H,

C*H*$_2$). ^{13}C NMR (125MHz, $CDCl_3$): δ 187.4, 182.1, 151.4, 151.2, 147.2, 136.1, 136.1, 132.0, 129.8, 124.4, 120.6, 119.5, 114.4, 94.0, 66.8, 49.5. HRMS (ESI) *m/z* 311.1390 $(M+H)^+$ calcd for $C_{18}H_{18}N_2O_3$, found 311.1389.

*1-(3-morpholinophenyl)-3-(pyridin-4-yl)propane-1,3-dione (**12**)*: Brown solid, Yield: 49%, ^{1}H NMR (400MHz, $CDCl_3$): δ 16.52 (s, 1H, O*H*), 8.80 (s, 2H, Py*H*), 7.82-7.81 (d, 2H, Py*H*), 7.55 (s, 1H, Ar*H*), 7.47-7.45 (d, 1H, Ar*H*), 7.41-7.38 (t, 1H, Ar*H*), 7.15-7.13 (d, 1H, Ar*H*), 6.86 (s, 1H, C=C*H*), 3.90-3.88 (m, 4H, C*H*$_2$), 3.26-3.23 (m, 4H, C*H*$_2$). ^{13}C NMR (100MHz, $CDCl_3$): δ 189.1, 180.3, 151.6, 150.0, 142.8, 136.2, 129.5, 120.6, 120.3, 119.0, 114.0, 94.4, 66.8, 49.0. HRMS (ESI) *m/z* 311.1390 $(M+H)^+$ calcd for $C_{18}H_{18}N_2O_3$, found 311.1393.

*1-(3-(4-methylpiperazin-1-yl)phenyl)-3-(pyridin-4-yl)propane-1,3-dione (**13**)*: Brown solid, Yield: 33%, ^{1}H NMR (400MHz, $CDCl_3$): δ 16.50 (s, 1H, O*H*), 8.81-8.79 (d, 2H, Py*H*), 7.79-7.77 (d, 2H, Py*H*), 7.56 (s, 1H, Ar*H*), 7.52-7.50 (d, 1H, Ar*H*), 7.43-7.39 (t, 1H, Ar*H*), 7.16-7.13 (d, 1H, Ar*H*), 6.85 (s, 1H, C=C*H*), 3.58-3.55 (m, 4H, C*H*$_2$), 3.05 (m, 4H, C*H*$_2$), 2.68 (s, 3H, C*H*$_3$). ^{13}C NMR (100MHz, $CDCl_3$): δ 189.1, 190.0, 151.5, 150.8, 142.4, 136.4, 129.6, 120.8, 120.5, 119.0, 114.7, 94.4, 54.9, 48.6, 45.9. HRMS (ESI) *m/z* 324.1707 $(M+H)^+$ calcd for $C_{19}H_{21}N_3O_2$, found 324.1708.

*1-(3-morpholinophenyl)-3-(p-tolyl)propane-1,3-dione (**18**)*: Yellow solid, Yield: 30%, ^{1}H NMR (400MHz, $CDCl_3$): δ 16.95 (s, 1H, O*H*), 7.90-7.88 (d, 2H, Ar*H*), 7.56 (s, 1H, Ar*H*), 7.47-7.45 (d, 1H, Ar*H*), 7.40-7.36 (t, 1H, Ar*H*), 7.30-7.28 (d, 2H, Ar*H*), 7.12-7.10 (d, 1H, Ar*H*), 6.81 (s, 1H, C=C*H*), 3.91-3.89 (m, 4H, C*H*$_2$), 3.26-3.23 (m, 4H, C*H*$_2$), 2.43 (s, 3H, C*H*$_3$). ^{13}C NMR

(100MHz, $CDCl_3$): δ 185.8, 185.6, 143.3, 136.7, 132.8, 129.4, 129.4, 127.2, 119.6, 118.8, 114.0, 93.0, 66.8, 49.2, 21.7. HRMS (ESI) *m/z* 324.1594 $(M+H)^+$ calcd for $C_{20}H_{21}NO_3$, found 324.1592.

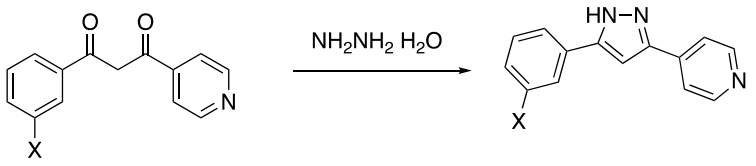

12 X = morpholine
13 X = 1-Me-piperazine

17 X = morpholine
15 X = 1-Me-piperazine

*General procedure for the syntheses of **15** and **17** (**17** as an example)*: 1-(3-morpholinophenyl)-3-(pyridin-4-yl)propane-1,3-dione (12) (31 mg, 0.1 mmol) and hydrazine monohydrate (0.1 mL) were refluxed in 10 mL of ethanol for 12 hours. The reaction mixture was then cooled to room temperature and concentrated in vacuo. The crude product was recrystallized from a dichloromethane/hexane mixture to obtain the final product as a white solid.

*1-methyl-4-(3-(3-(pyridin-4-yl)-1H-pyrazol-5-yl)phenyl)piperazine (**15**)*: White solid, Yield: 99%, ^{1}H NMR (500MHz, DMSO-d_6): δ 13.57 (s, 1H, N*H*), 8.62-8.61 (d, 2H, Py*H*), 7.81-7.80 (d, 2H, Py*H*), 7.39 (s, 2H, Ar*H* and C=C*H*(Hpz)), 7.31-7.28 (t, 1H, Ar*H*), 7.23 (d, 1H, Ar*H*), 6.94-6.93 (d, 1H, Ar*H*), 3.23-3.21 (m, 4H, CH_2), 2.50-2.48 (m, 4H, CH_2), 2.24 (s, 3H, CH_3). ^{13}C NMR (125MHz, DMSO-d_6): δ 151.9, 150.6, 130.1, 119.9, 116.1, 115.6, 112.3, 101.2, 55.0, 48.3, 46.2. HRMS (ESI) *m/z* 320.1870 $(M+H)^+$ calcd for $C_{19}H_{21}N_5$, found 320.1879.

*4-(3-(3-(pyridin-4-yl)-1H-pyrazol-5-yl)phenyl)morpholine (**17**)*: White solid, Yield: 99%, ^{1}H NMR (500MHz, DMSO-d_6): δ 13.56 (s, 1H, N*H*), 8.62-8.61 (d, 2H, Py*H*), 7.81-7.80 (d, 2H, Py*H*), 7.39 (s, 2H, Ar*H* and C=C*H*(Hpz)), 7.34-7.31 (t, 1H, Ar*H*), 7.27-7.26 (d, 1H, Ar*H*), 6.96-

6.94 (d, 1H, Ar*H*), 3.79-3.77 (m, 4H, CH_2), 3.21-3.19 (m, 4H, CH_2). ^{13}C NMR (125MHz, DMSO-d_6): δ 151.5, 150.2, 129.6, 119.4, 116.1, 114.9, 111.7, 101.0, 66.1, 48.3. HRMS (ESI) *m/z* 307.1553 $(M+H)^+$ calcd for $C_{18}H_{18}N_4O$, found 307.1561.

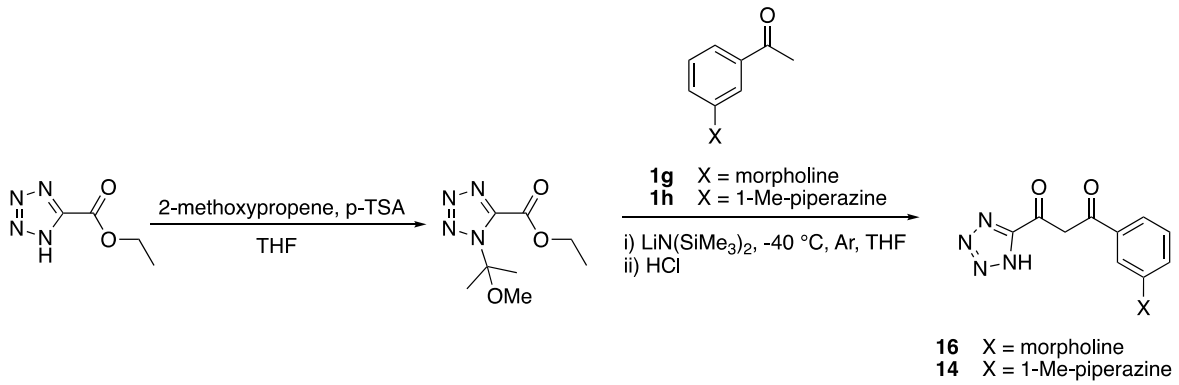

General procedure for the syntheses of ***14*** *and* ***16*** *(****16*** *as an example)*: Ethyl 1*H*-tetrazolium-5-carboxylate (213 mg, 1.5 mmol), p-toluenesulfonic acid monohydrate (3 mg, 0.015 mmol), and 2-methoxypropene (0.16 mL, 1.65 mmol) were dissolved in 5 mL of THF and stirred at room temperature for 1 hour to obtain *Mixture 1*.

In a separate flask, 1-(3-morpholinophenyl)ethan-1-one (**1g**) (308 mg, 1.5 mmol) was placed, and the flask was evacuated and backfilled with Ar. THF (5 mL) was added to the flask and cooled to -40 ºC. $LiN(SiMe_3)_2$ (1.0 M in THF) (3.3 mL, 3.3 mmol) was then slowly added dropwise to the solution over 20 minutes. The mixture was stirred at -40 ºC for 10 minutes to obtain *Mixture 2*.

Mixture 2 was then slowly added dropwise to *Mixture 1* and stirred at room temperature for 6 hours. The reaction mixture was then dried in vacuo, and diethyl ether (30 mL) was added. The resulting precipitate was filtered and dissolved in 50 mL of water. 6 N HCl was then slowly added dropwise with constant swirling until yellow precipitates started to form. The mixture flask

was then placed in an ice bath for 3 hours. The resulting precipitates were filtered and dried to obtain the final product as an orange solid.

*1-(3-(4-methylpiperazin-1-yl)phenyl)-3-(1H-tetrazol-5-yl)propane-1,3-dione (**14**)*: Yellow solid, Yield: 15%, ^{1}H NMR (500MHz, DMSO-d_6): δ 10.67 (s, 1H, N*H*), 7.64 (s, 1H, Ar*H*), 7.59-7.58 (d, 1H, Ar*H*), 7.50-7.47 (t, 1H, Ar*H*), 7.44 (s, 1H, C=C*H*), 7.35-7.34 (d, 1H, Ar*H*), 4.00-3.17 (m, 8H, CH_2), 2.83 (s, 3H, CH_3). ^{13}C NMR (125MHz, DMSO-d_6): δ 186.1, 174.0, 150.5, 135.0, 130.5, 121.6, 119.4, 114.6, 96.9, 52.5, 45.7, 42.4. HRMS (ESI) *m/z* 315.1564 $(M+H)^+$ calcd for $C_{15}H_{18}N_6O_2$, found 315.1570.

*1-(3-morpholinophenyl)-3-(1H-tetrazol-5-yl)propane-1,3-dione (**16**)*: Yellow solid, Yield: 13%, ^{1}H NMR (500MHz, DMSO-d_6): δ 7.53-7.52 (d, 1H, Ar*H*), 7.51 (s, 1H, Ar*H*), 7.45-7.42 (t, 1H, Ar*H*), 7.33 (s, 1H, C=C*H*), 7.29-7.27 (d, 1H, Ar*H*), 3.77-3.75 (m, 4H, CH_2), 3.21-3.20 (m, 4H, CH_2). ^{13}C NMR (125MHz, DMSO-d_6): δ 186.3, 173.8, 152.0, 134.6, 130.3, 121.0, 118.7, 113.4, 96.7, 66.5, 48.6. HRMS (ESI) *m/z* 324.1067 $(M+Na)^+$ calcd for $C_{14}H_{15}N_5O_3$, found 324.1069.

1-2. Protein purification and in vitro enzymatic activity assay

§ *Given that LH2b, the longer LH2 isoform that includes exon 13A, promotes metastasis and cancer progression, while LH2a does not,[4] we used LH2b as the representative form of LH2 in this study, and LH2 will refer to LH2b unless otherwise specified.*

Human LH1-3 recombinant proteins were purified from CHO cell-derived conditioned medium samples as described previously.[1] LH1-3 expression vectors were transiently transfected in new Gibco™ ExpiCHO™ cells (Thermo Fisher Scientific, Waltham, MA) with polyethylenimine and expressed as a secreted protein with N-terminal His_8 and human growth hormone (hGH) tags. The LH1-3–containing conditioned medium samples were harvested by centrifugation at 7,000 rpm for 10 min, filtered through 0.22 μm EMD Millipore Stericup™ Sterile Vacuum Filter Units (EMD Millipore, Billerica, MA), concentrated and buffer-exchanged into Nickel-binding buffer (20 mM Tris, pH 8.0, 200 mM NaCl, 15 mM imidazole) using the Centramate™ & Centramate PE Lab Tangential Flow System (Pall Life Sciences, Ann Arbor, MI). The recombinant LH proteins were purified with immobilized metal affinity and anion exchange chromatography.

LH enzymatic activity was measured using a luciferase-based assay as described.[2] In brief, the assay was performed in LH reaction buffer (50 mM HEPES pH 7.4, 150 mM NaCl) at 37 °C for 1 h with 1 μM LH enzymes, 10 μM $FeSO_4$, 100 μM 2-OG, 500 μM ascorbate, 1 mM DTT, 0.01% triton x-100, and 1 mM IKGIKGIKG collagen telopeptide mimics. Except for LH recombinant proteins, all reagents were prepared immediately before use. All reagents were dissolved in reaction buffer except for $FeSO_4$, which was prepared in 10 mM HCl, and the pH of the reaction mixture was checked with pH papers to ensure that HCl did not change the overall sample pH. All compounds were pre-incubated with LHs at RT for 30 min before LH enzymatic activity assay. LH activity was measured by detecting succinate production with Succinate-Glo™ kit reagents (Succinate-Glo™ JmjC Demethylase/Hydroxylase Assay, Promega, Madison, WI) according to manufacturers' instructions. Experiments were performed in triplicates, and IC_{50}

values were determined by fitting the data using four-parameter logistic regression in SigmaPlot 14.5.

1-3. Selectivity test over other Fe(II)/2OG-dependent enzymes

Human EGLN1 (NP_071334.1) and human FTO (XP_011521615.1) were purchased from Active Motif (cat# 81065 and 31572, respectively). The substrate for EGLN1 (pepEGLN1) was a peptide of HIF-1α residues 556-574 and purchased from Anaspec (cat# AS-61528, DLDLEALAPYIPADDDFQL). The FTO substrate (oligoFTO, 5'-rCrUrU rGrUrC rA/iN6Me-rA/rC rArGrC rArGrA-3') was custom synthesized from Integrated DNA Technologies. JMJD2A (HDM) was a gift from Dr. Martinez at the University of Texas Southwestern Medical Center, and its substrate peptide H3K9me3 was purchased from Cayman (Cat# 10530, ARTKQTARK$(Me)_3$-STGGKA) respectively. L230 protein was synthesized as reported previously[3], and its peptide substrate (GTKGETGLKGII, abbreviated pepL230) was procured from LifeTein. All tested compounds were dissolved in DMSO to form 10 mM stock solutions.

With little modification, selectivity tests were conducted similarly to the activity assay described above. Assays were performed in 50 mM HEPES, pH 7.5, containing 10 μg/mL BSA, 0.01 % Tween-20, 1 mM DTT, 10 μM $FeCl_2$, and 100 μM ascorbate. Briefly, 2.5 μL of 5X compounds were incubated with 5 μL of 2.5X enzyme for 30 min at RT. Compounds **6**, **12**, and **13** were each tested at a final concentration of 11 μM. Enzymatic activity assays were initiated by adding 5 μL 2.5X substrate mixture (2OG with or without each appropriate enzyme-specific substrate). The final concentrations of the enzymes were 1 μM HDM, 0.2 μM EGLN1, 0.5 μM FTO, 1 μM LH2 and 1 μM L230, respectively. Enzyme-specific substrate concentrations were either 6 μM (H3K9me3, pepEGLN1, oligoFTO) or 1 mM (IKGIKGIKG, pepL230), and all reactions contained the additional substrate 2OG at a final concentration of 10 μM. Reactions proceeded for 1 h at RT, followed by processing with the Succinate-Glo™ kit according to

manufacturer instructions. Glo kit reagents were supplemented with 0.01% Tween-20. Luminescence measurements were collected on a Synergy Neo2 multi-mode plate reader (Agilent) with all samples in 384-well white polystyrene plates (Corning, cat# 3825).

1-4. Cell culture

The murine lung cancer cell lines 344SQ[58] and 344SQ LH2KO were provided by J. M. Kurie (Department of Thoracic/ Head and Neck Medical Oncology at MD Anderson). 344SQ and 344SQ LH2KO cells were cultured in RPMI 1640 (Corning) containing 10% fetal bovine serum (Gibco) for growth or maintenance. Cultures were incubated at 37°C in a humidified 5% CO_2 incubator and supplemented with penicillin (100 U) and streptomycin (100 μg/ml; Invitrogen). LH2KO 344SQ cells were generated using a previously published protocol.[4]

1-5. Migration assay

The migration assay was done in 8.0 μm Boyden Chambers (Corning). Briefly, 20,000 cells were resuspended in 200 μL FBS-free RPMI 1640 (Corning) containing varying concentrations of compound **13,** and the cells were plated in the inner portion of the chambers. RPMI 1640, containing 10 % FBS, was added to the outer portion of the chambers. After incubating overnight, the cells in the chambers were harvested and washed with PBS. To fix the cells on the chamber membrane, the chambers were immersed in 90% ethanol for 20 min. Then the chambers were immersed in 0.1% crystal violet for 10 min. After staining, the chambers were dried and taken representative images for cell counting.

1-6. Proliferation assay

Two thousand cells were resuspended in RPMI1640 containing 10% FBS and plated into 96-well plates. After overnight incubation, the medium was replaced with fresh medium containing varying concentrations of Compound **13**. After 48 hours of treatment, the relative cell proliferation was measured using the CCK-8 kit (APExBIO) following the protocol.

1-7. Computational methods

The preparation of the systems, molecular docking, polarizable molecular dynamics simulations (MD), clustering analysis, polarizable quantum mechanics/molecular mechanics interaction energy calculations ($IE_{QM/MM}$), and the non-covalent interactions (NCI) analyses have been explained in detail previously.[5] Briefly, the SWISS-MODEL server[6] was used to construct the homology model for LH2. After performing 1 ns of equilibration, 5 ns of polarizable MD production simulations were performed under NPT ensemble using the Tinker software[7] (Figure S39). The MD trajectories for each structure were then used for a six-dimensional clustering analysis via the *k*-means algorithm[8] (see Figures S41–S46 and Table S1). Each dimension in this analysis corresponds to a distance between the iron and the donor atoms of the coordinated residues ligand, a water molecule (in compounds **6** and **12**), two histidine residues, and an aspartate (see Figure S40). The relative QM/MM optimization energies were calculated for each representative of the clusters (see Table S1), and the representative with the lowest relative optimization energy and the highest percentage in the cluster was used for calculating QM/MM interaction energies ($IE_{QM/MM}$ in Table S2). The QM/MM calculations were carried out using LICHEM[9-10], combining

Gaussian16[11] and TINKER.[12] The ωB97X-D/6–31G(d,p)[13-14] level of theory and AMOEBAbio18[15] force field were employed for the QM subsystem and the MM region of the calculations, respectively. Multiwfn[16] was employed to analyze the non-covalent interactions (NCI) between the ligand and the surrounding amino acid residues and solvent/molecular fragments using the promolecular density method.[17] Visual molecular dynamics (VMD) was used to create images and visualize the isosurface values.[18] The isovalue for the NCI visualization is 0.4 au with the color scale of -0.05 au $< \text{sign}(\lambda_2)\rho < 0.05$ au. Intramolecular tunnel analysis was performed and illustrated with Caver Analyst 2.0[19-20] to calculate the possibility of O_2-transporting tunnels in systems with compounds **6**, **12**, and **13**.

2. NMR spectra

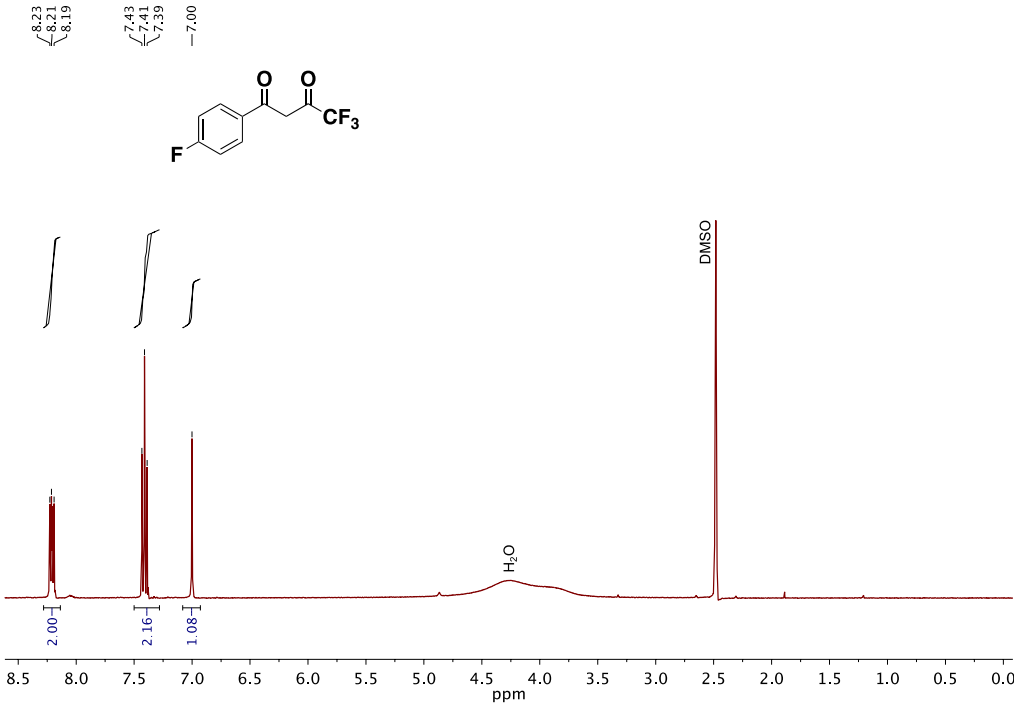

Figure S1. ^{1}H-NMR spectrum of **3** recorded in DMSO-d_6.

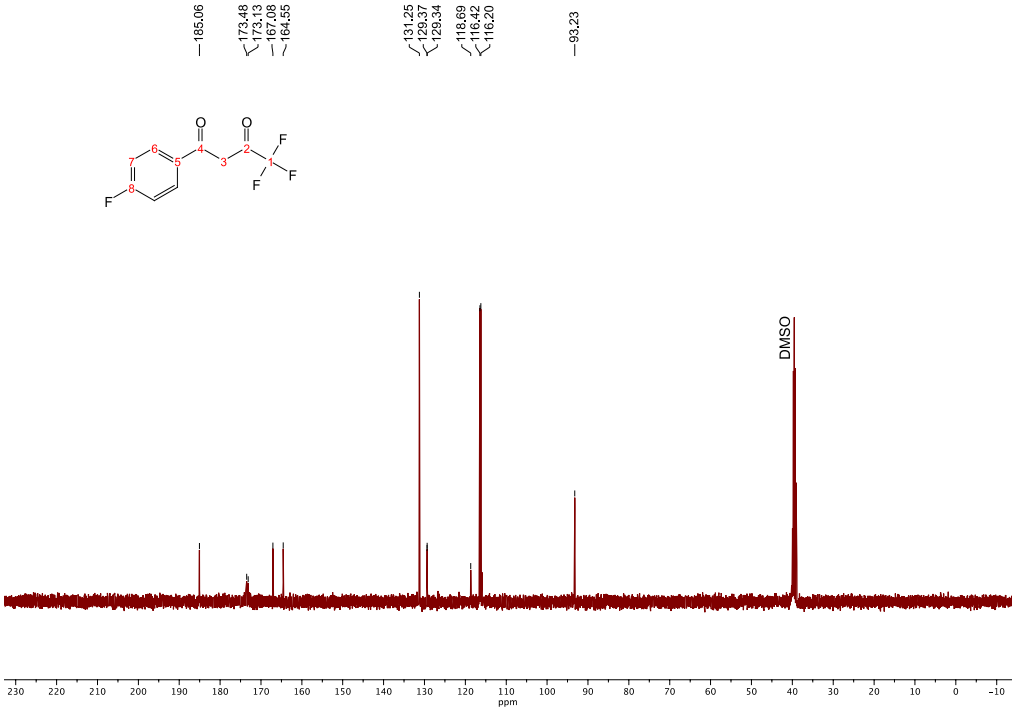

Figure S2. ^{13}C-NMR spectrum of **3** recorded in DMSO-d_6.

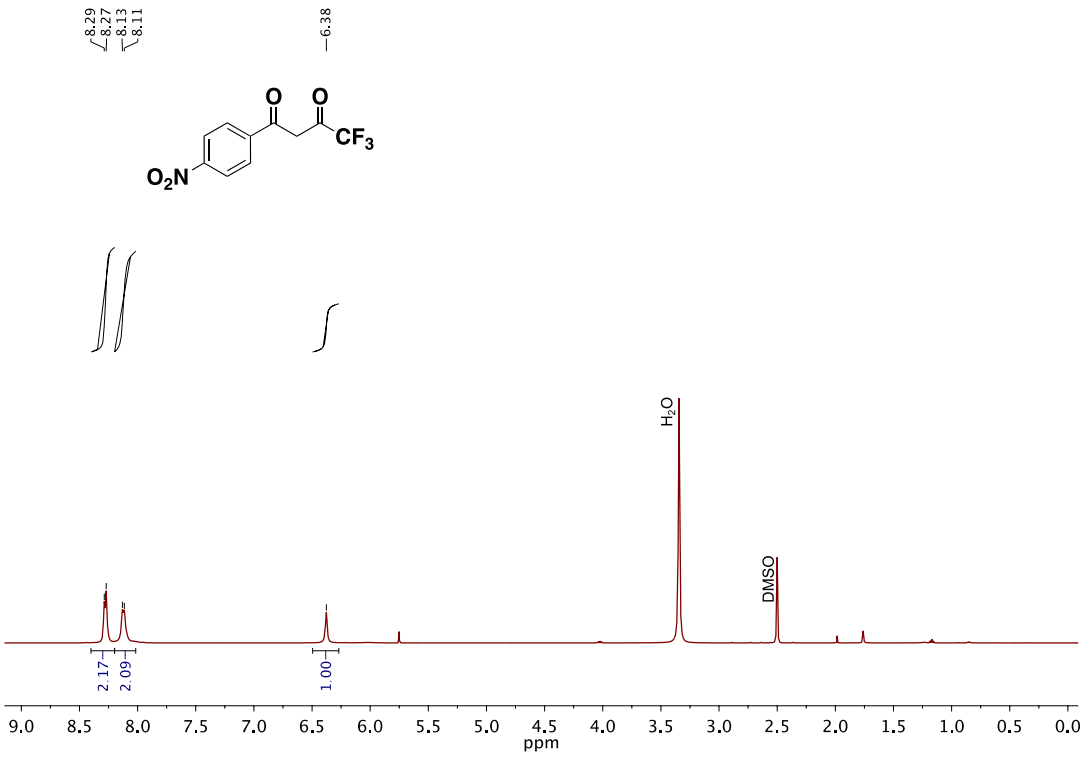

Figure S3. [1]H-NMR spectrum of **4** recorded in DMSO-d_6.

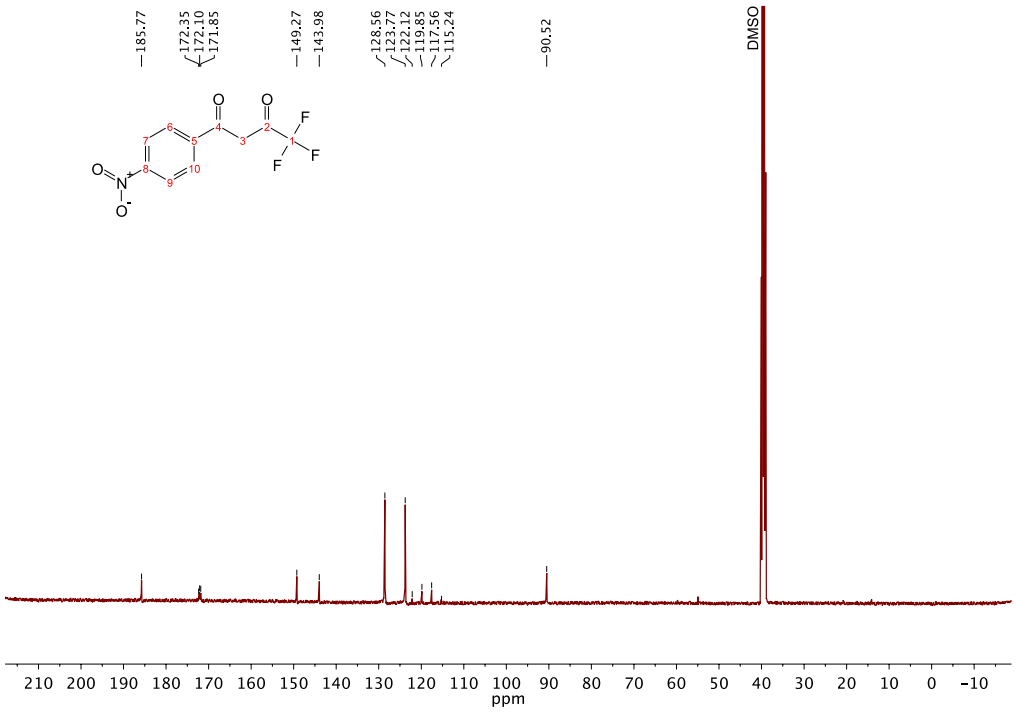

Figure S4. [13]C-NMR spectrum of **4** recorded in DMSO-d_6.

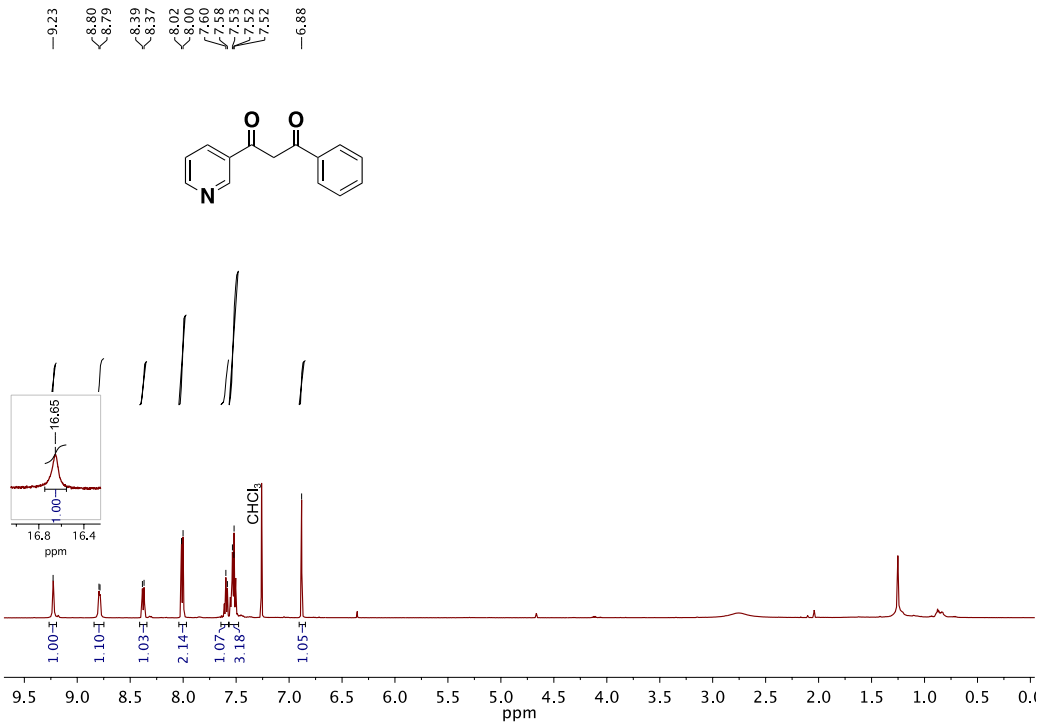

Figure S5. ^{1}H-NMR spectrum of **5** recorded in $CDCl_3$.

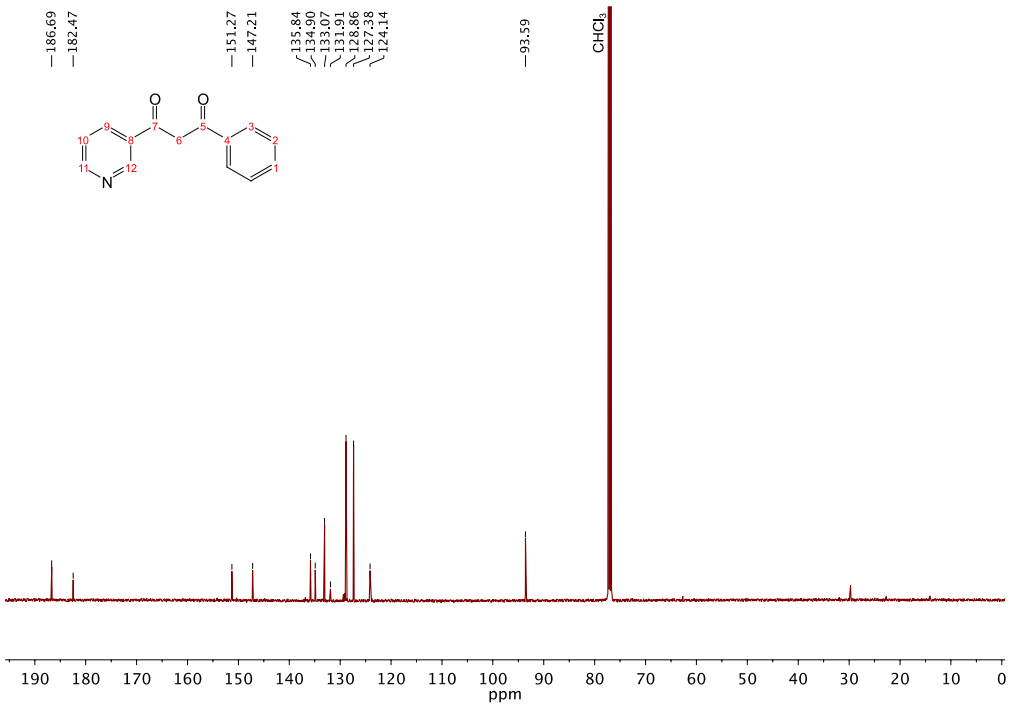

Figure S6. ^{13}C-NMR spectrum of **5** recorded in $CDCl_3$.

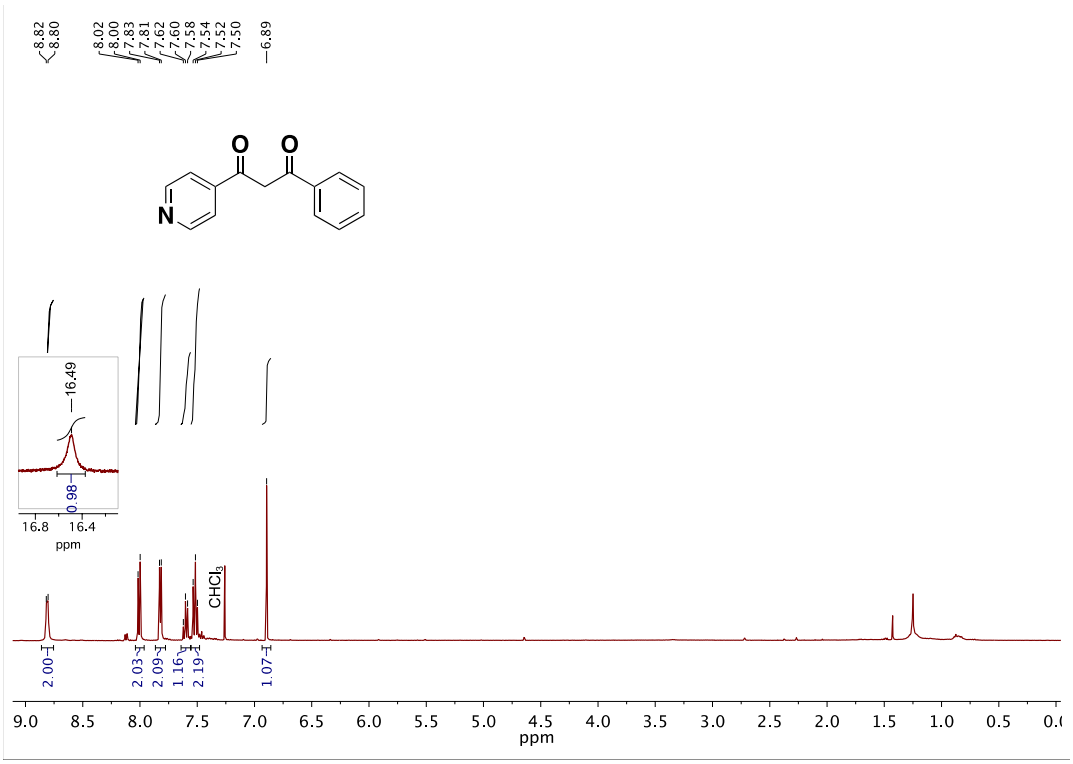

Figure S7. ^{1}H-NMR spectrum of **6** recorded in $CDCl_3$.

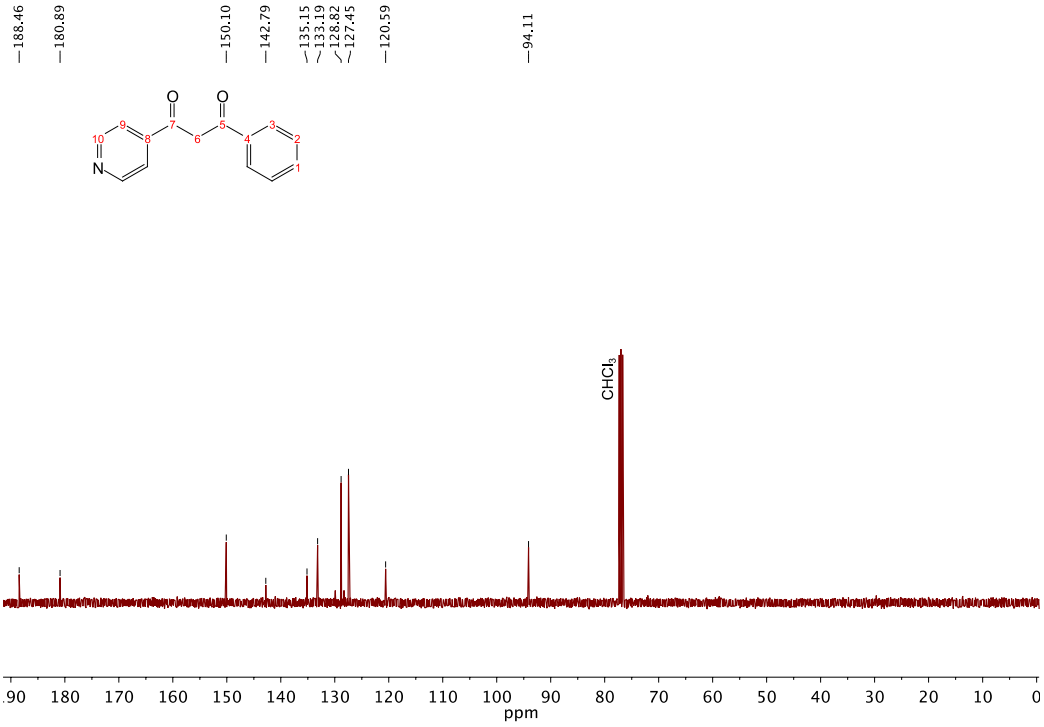

Figure S8. ^{13}C-NMR spectrum of **6** recorded in $CDCl_3$.

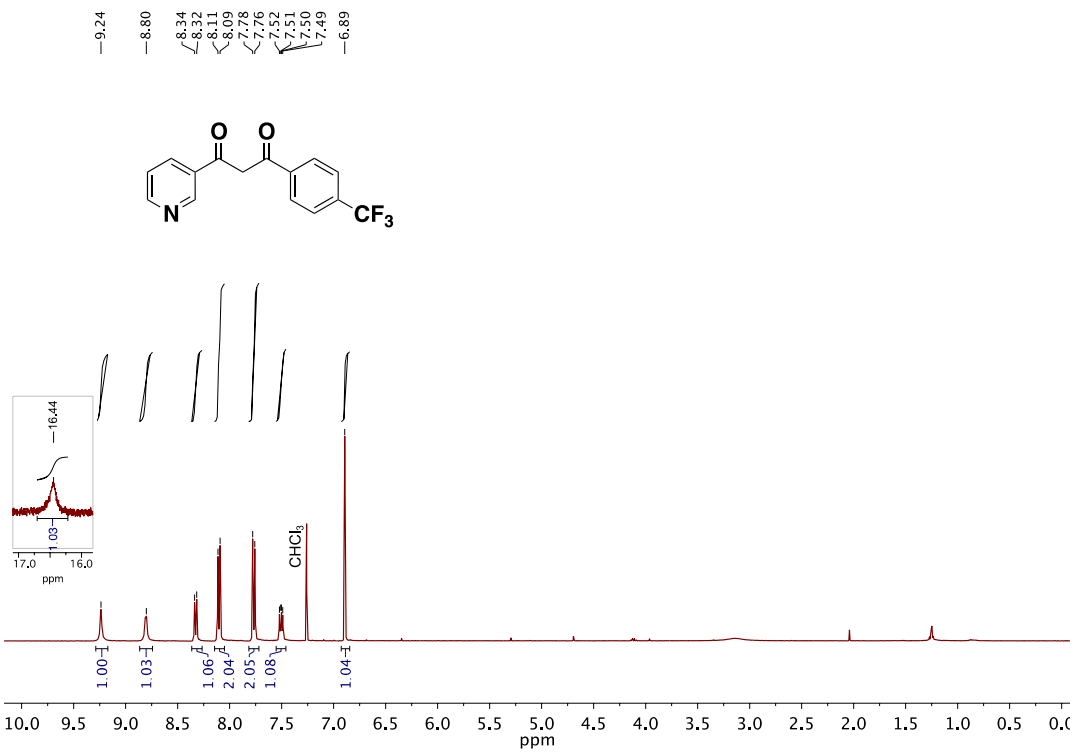

Figure S9. ^{1}H-NMR spectrum of **7** recorded in $CDCl_3$.

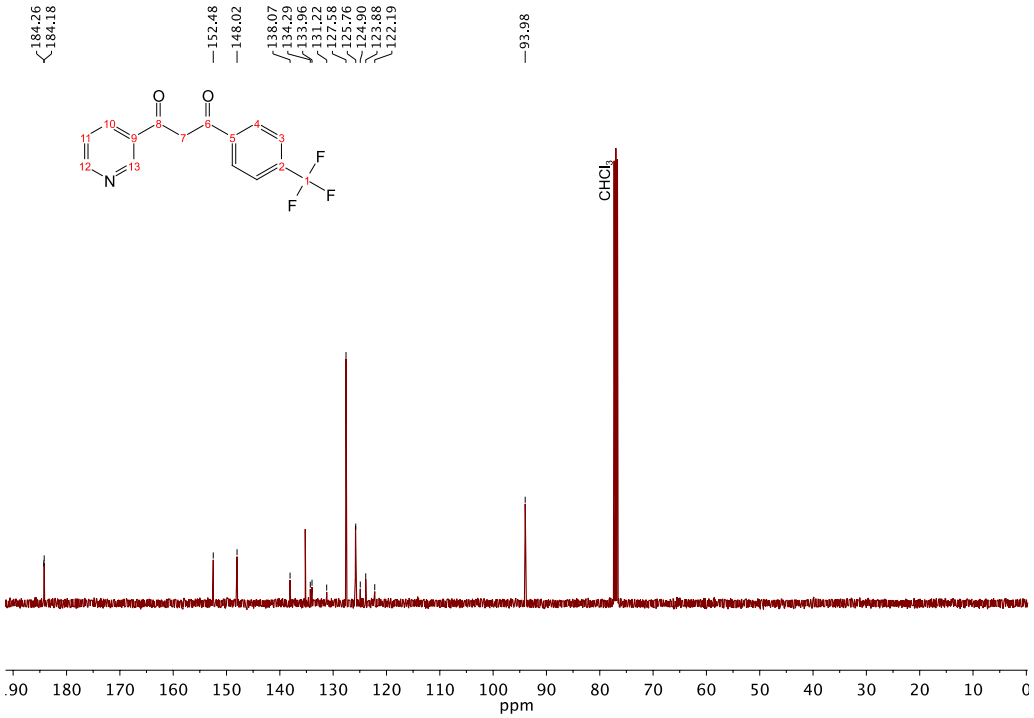

Figure S10. ^{13}C-NMR spectrum of **7** recorded in $CDCl_3$.

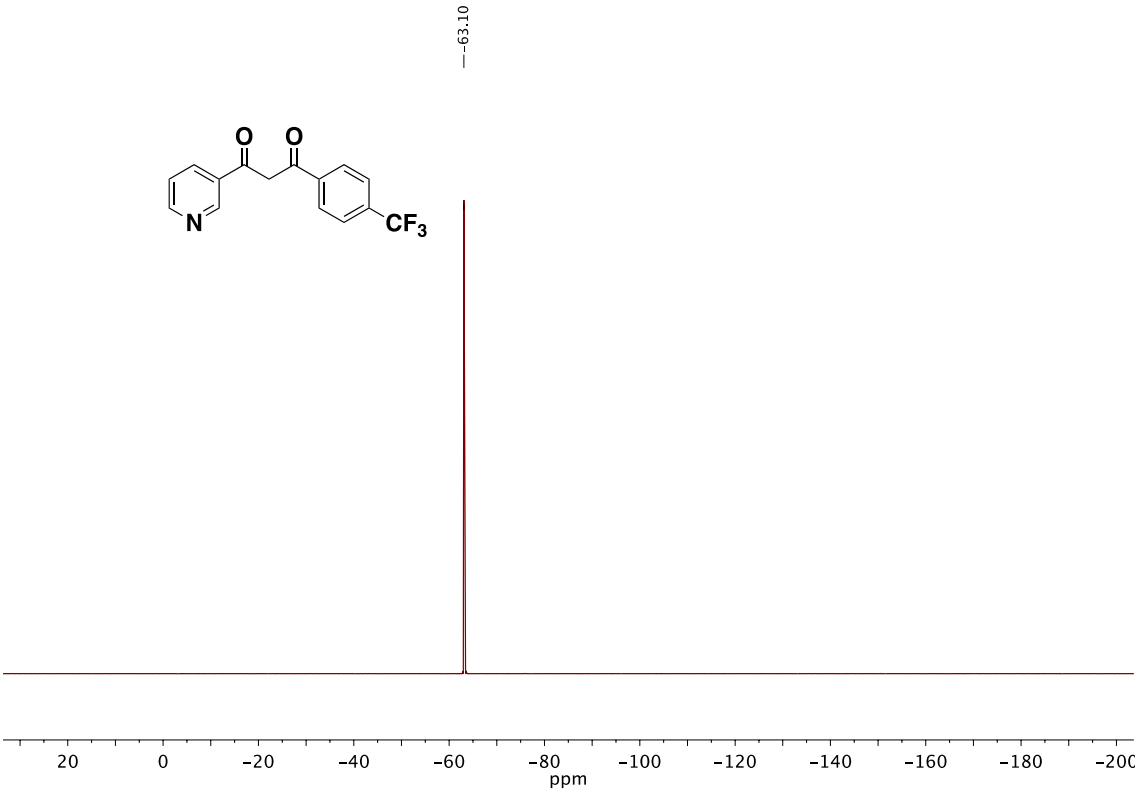

Figure S11. ^{19}F-NMR spectrum of **7** recorded in $CDCl_3$.

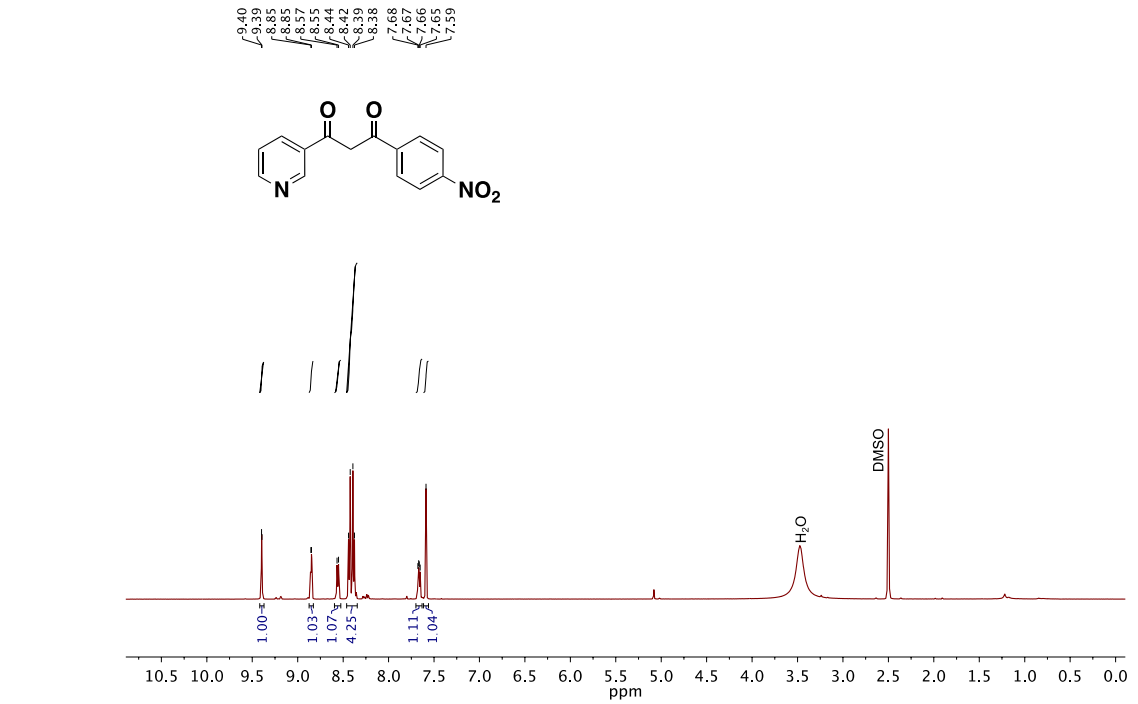

Figure S12. ^{1}H-NMR spectrum of **8** recorded in DMSO-d_6.

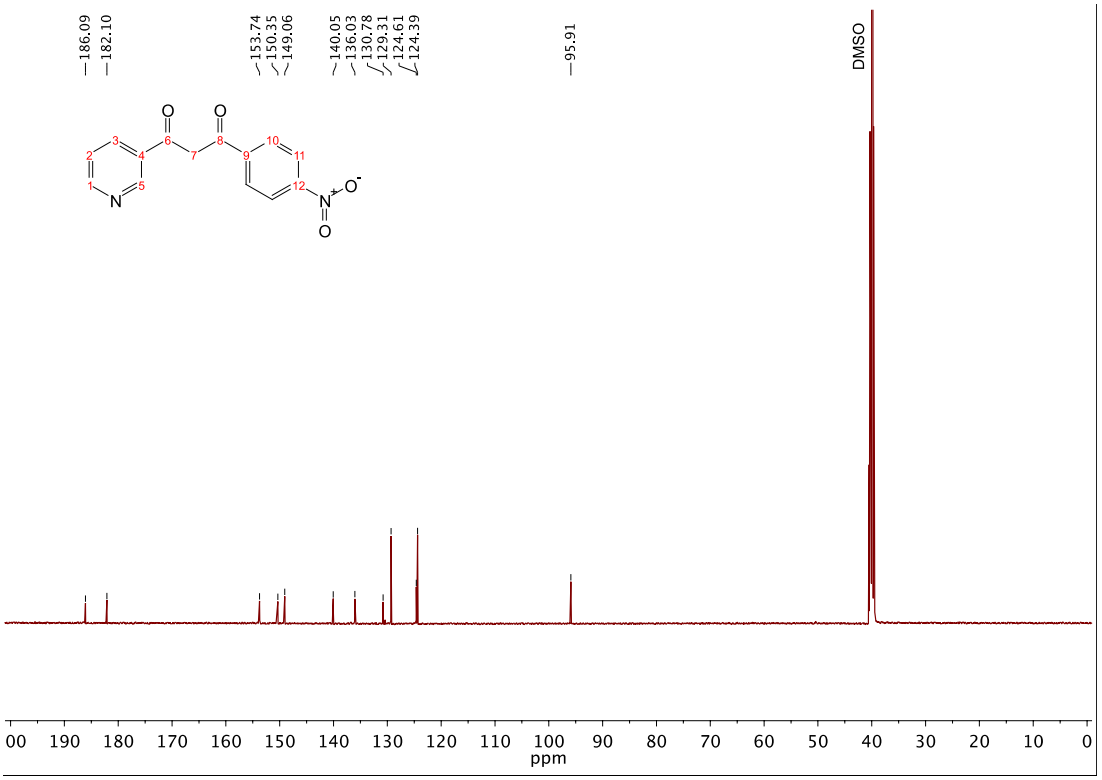

Figure S13. ^{13}C-NMR spectrum of **8** recorded in DMSO-d_6.

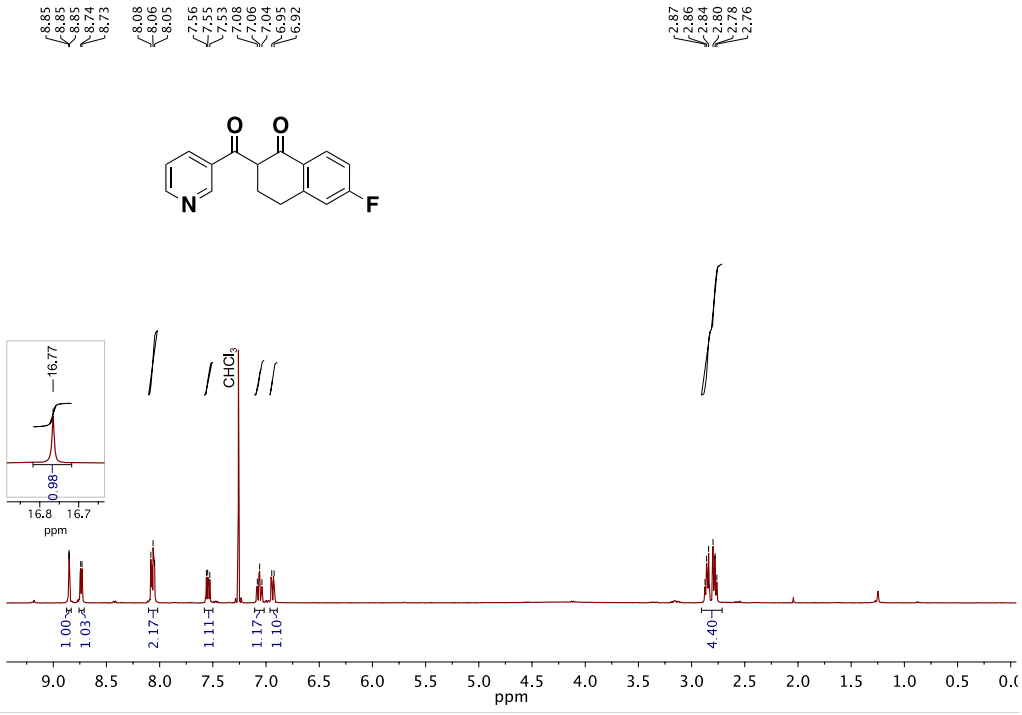

Figure S14. ^{1}H-NMR spectrum of **9** recorded in $CDCl_3$.

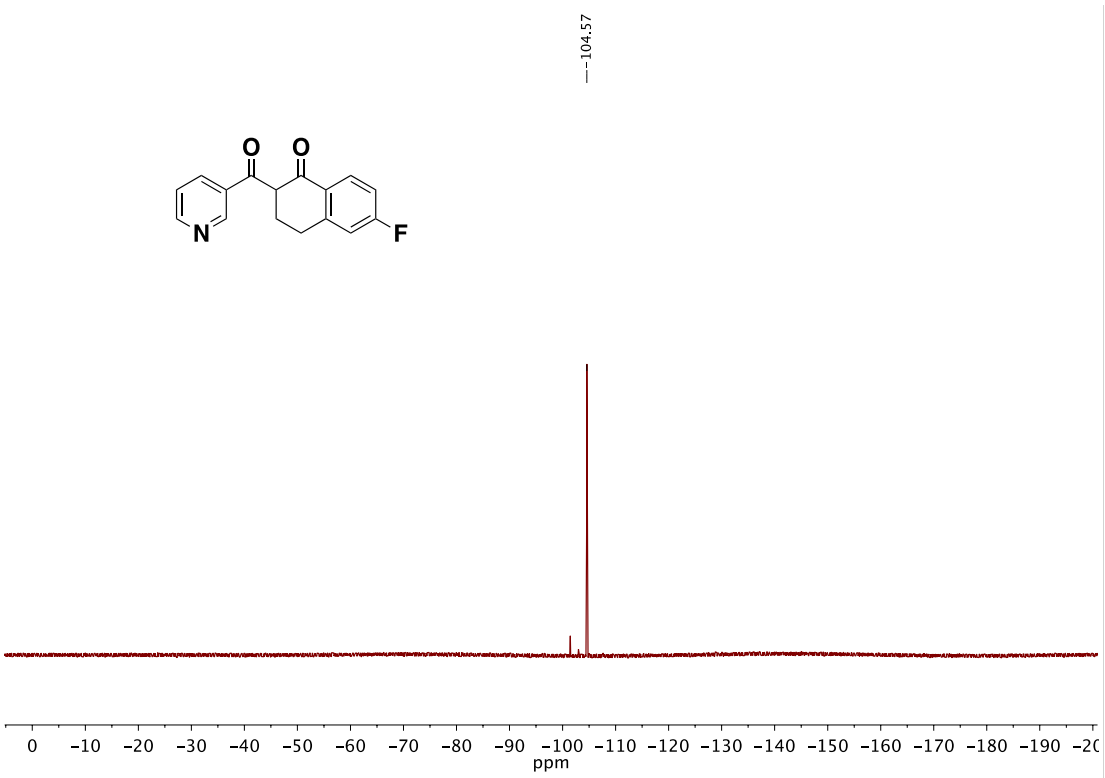

Figure S15. ^{19}F-NMR spectrum of **9** recorded in $CDCl_3$.

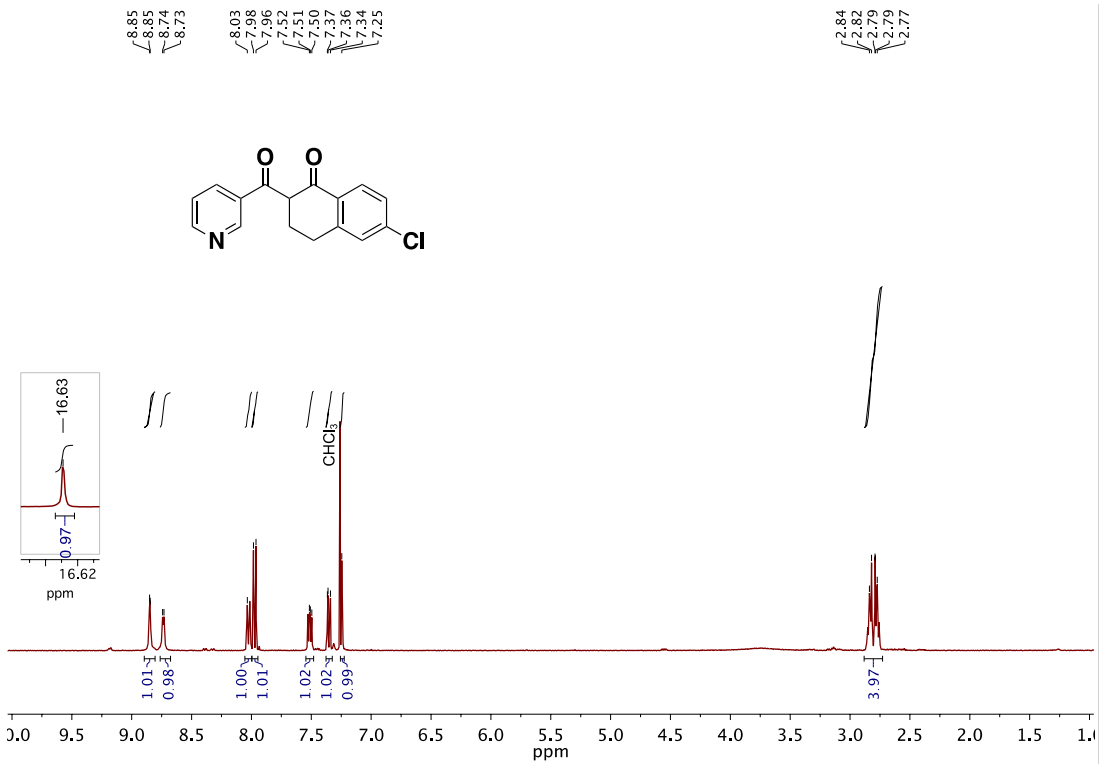

Figure S16. ^{1}H-NMR spectrum of **10** recorded in $CDCl_3$.

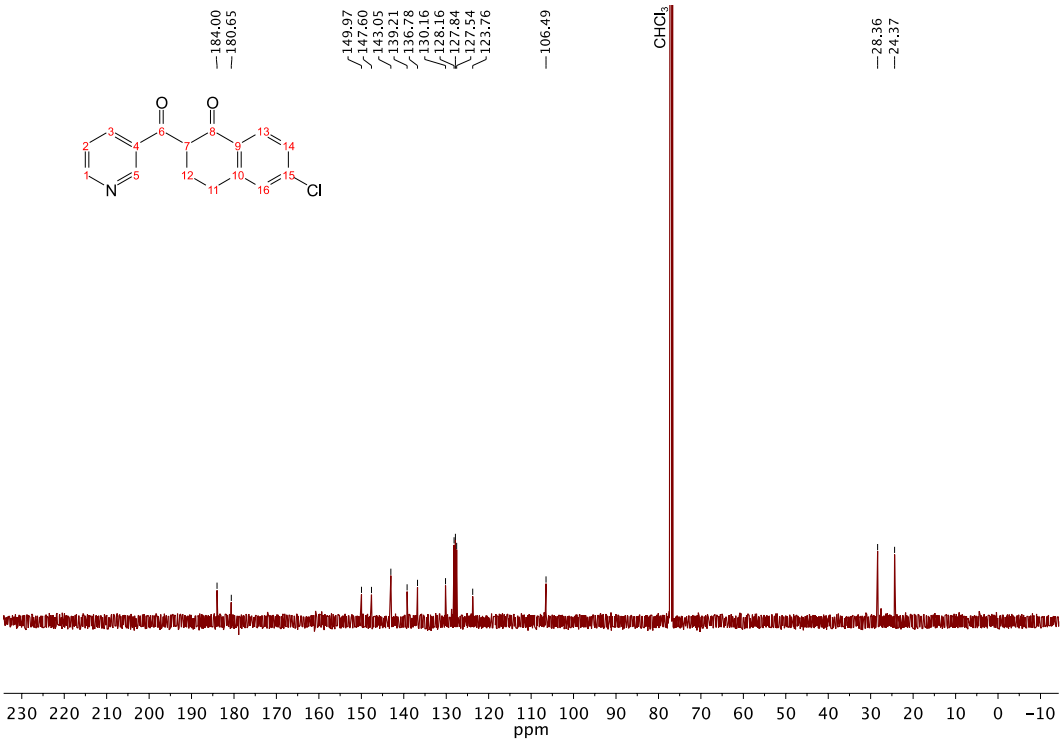

Figure S17. ^{13}C-NMR spectrum of **10** recorded in $CDCl_3$.

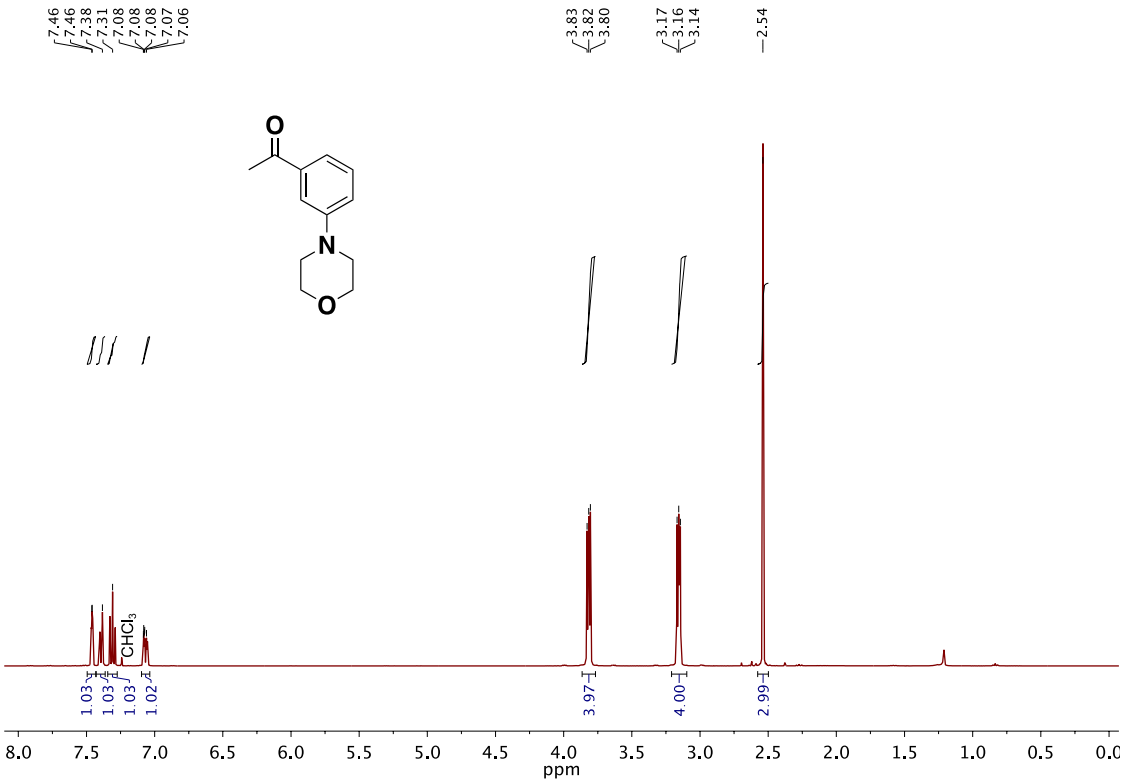

Figure S18. ^{1}H-NMR spectrum of **1g** recorded in $CDCl_3$.

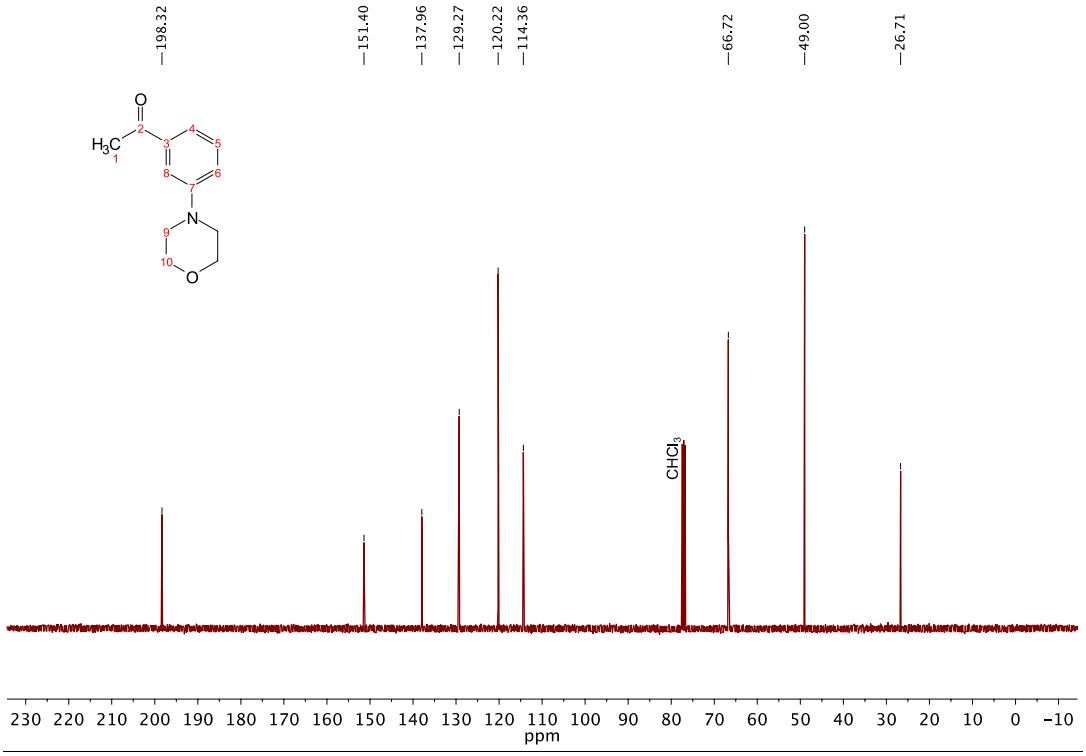

Figure S19. ^{13}C-NMR spectrum of **1g** recorded in $CDCl_3$.

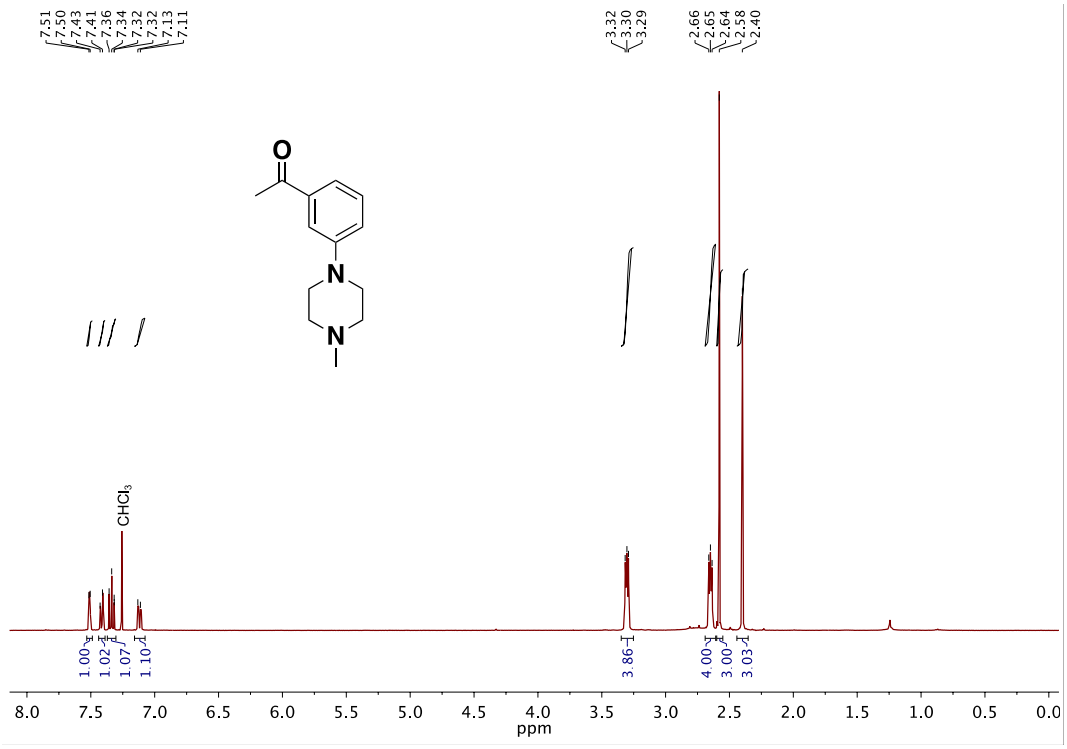

Figure S20. ^{1}H-NMR spectrum of **1h** recorded in $CDCl_3$.

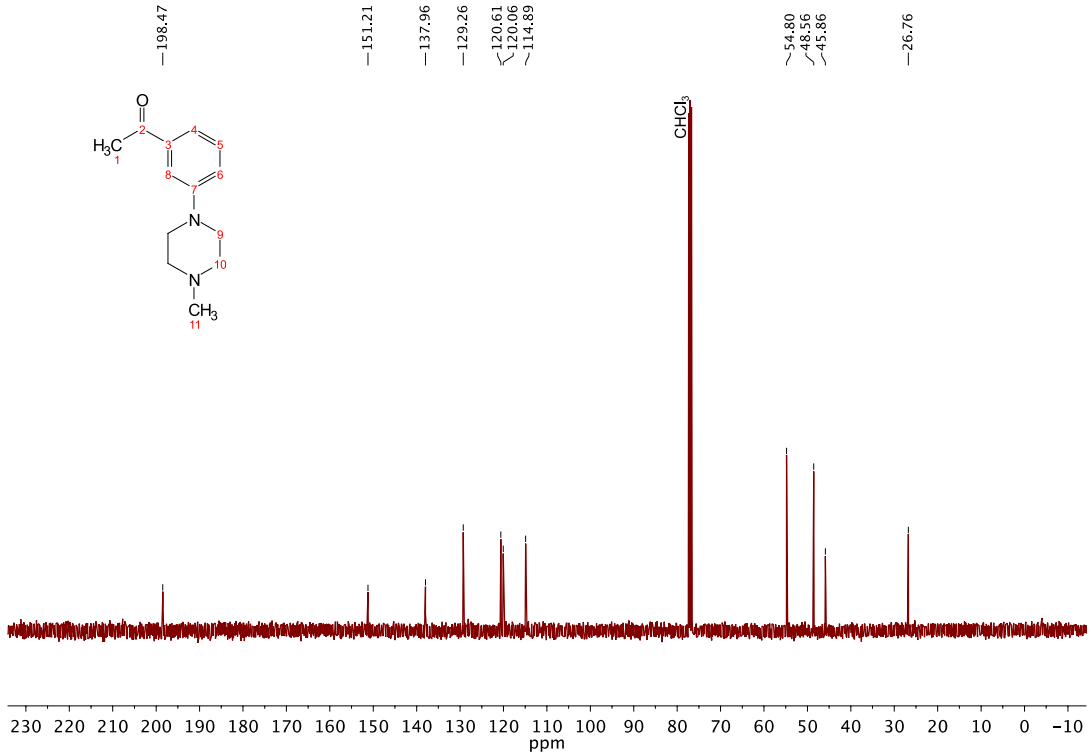

Figure S21. ^{13}C-NMR spectrum of **1h** recorded in $CDCl_3$.

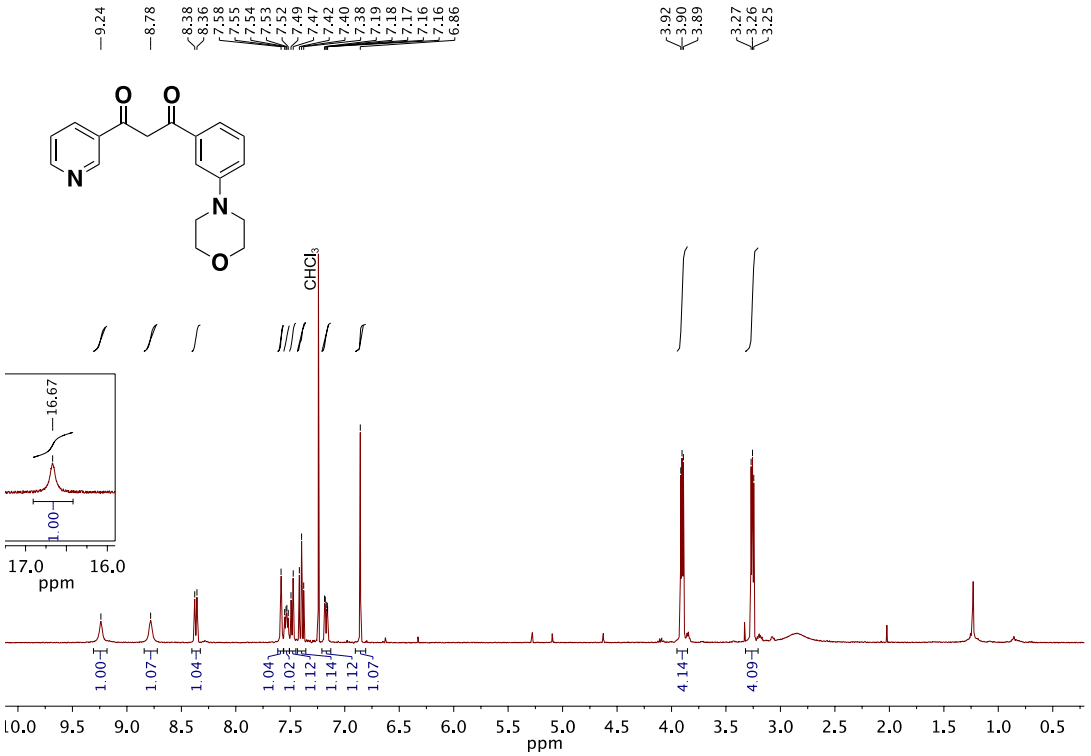

Figure S22. ^{1}H-NMR spectrum of **11** recorded in $CDCl_3$.

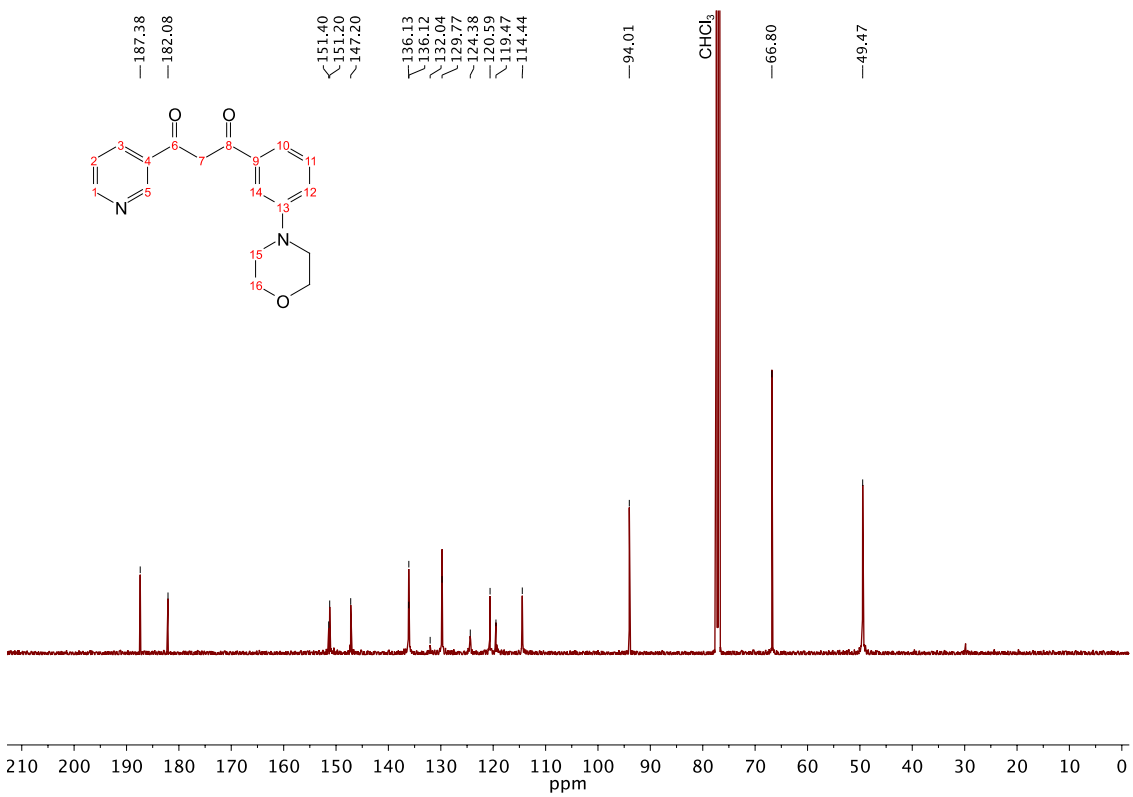

Figure S23. ^{13}C-NMR spectrum of **11** recorded in $CDCl_3$.

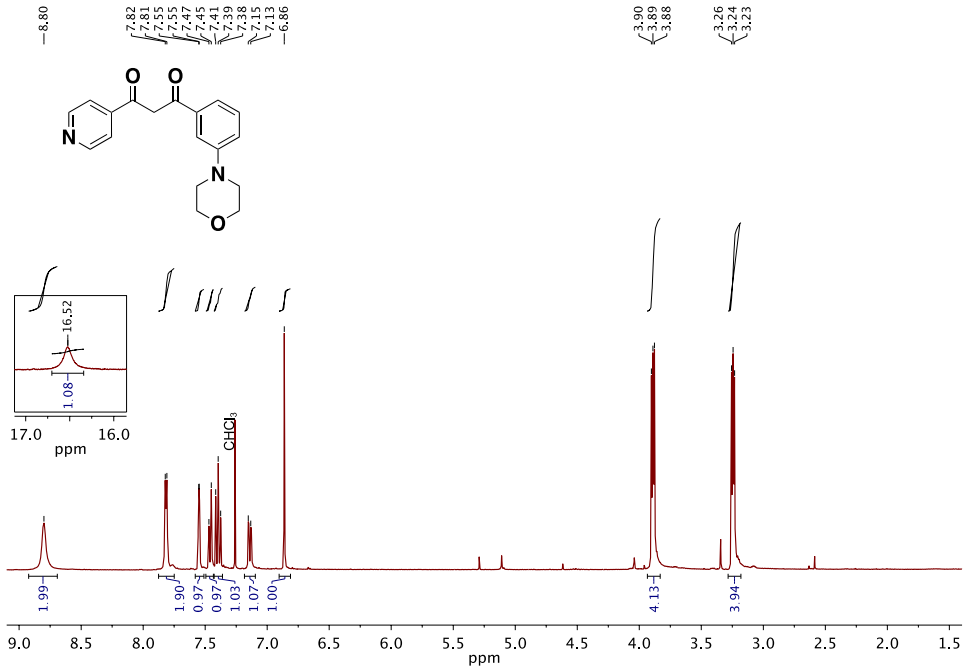

Figure S24. ^{1}H-NMR spectrum of **12** recorded in $CDCl_3$.

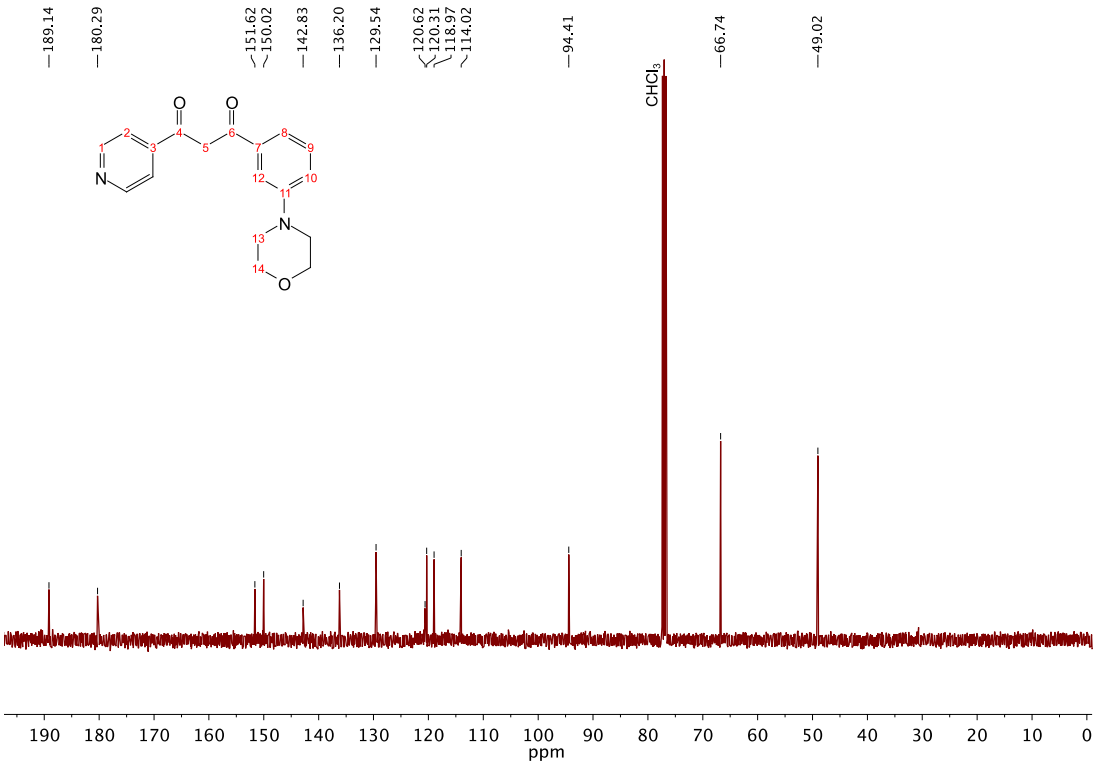

Figure S25. ^{13}C-NMR spectrum of **12** recorded in $CDCl_3$.

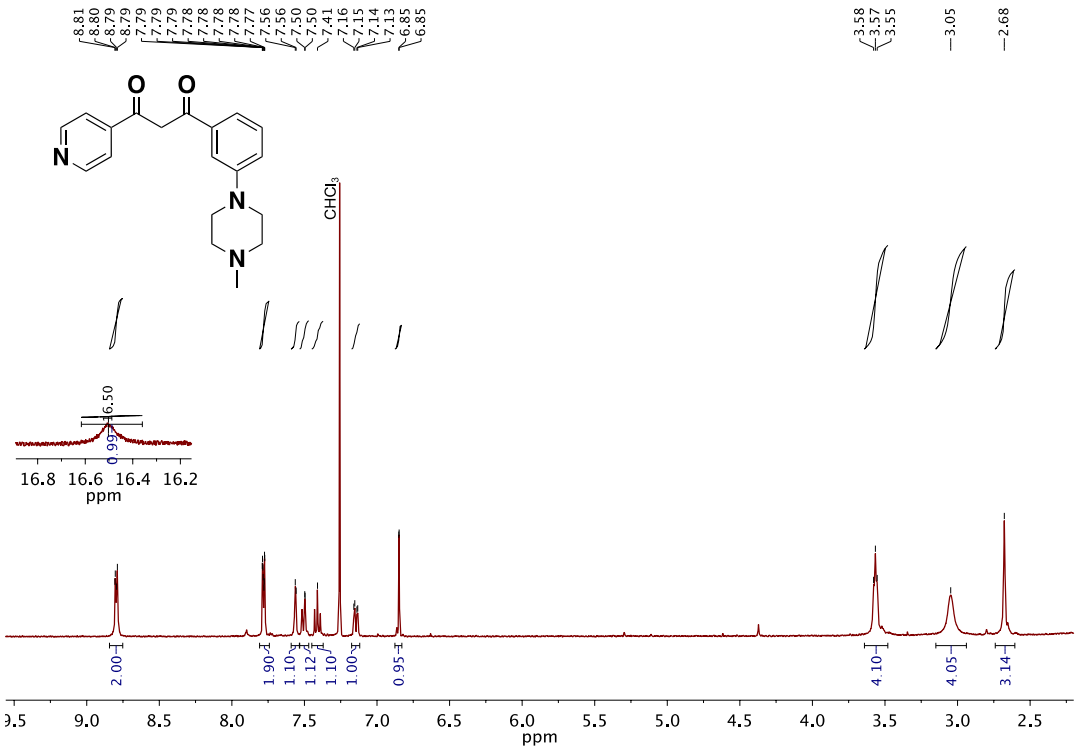

Figure S26. ^{1}H-NMR spectrum of **13** recorded in $CDCl_3$.

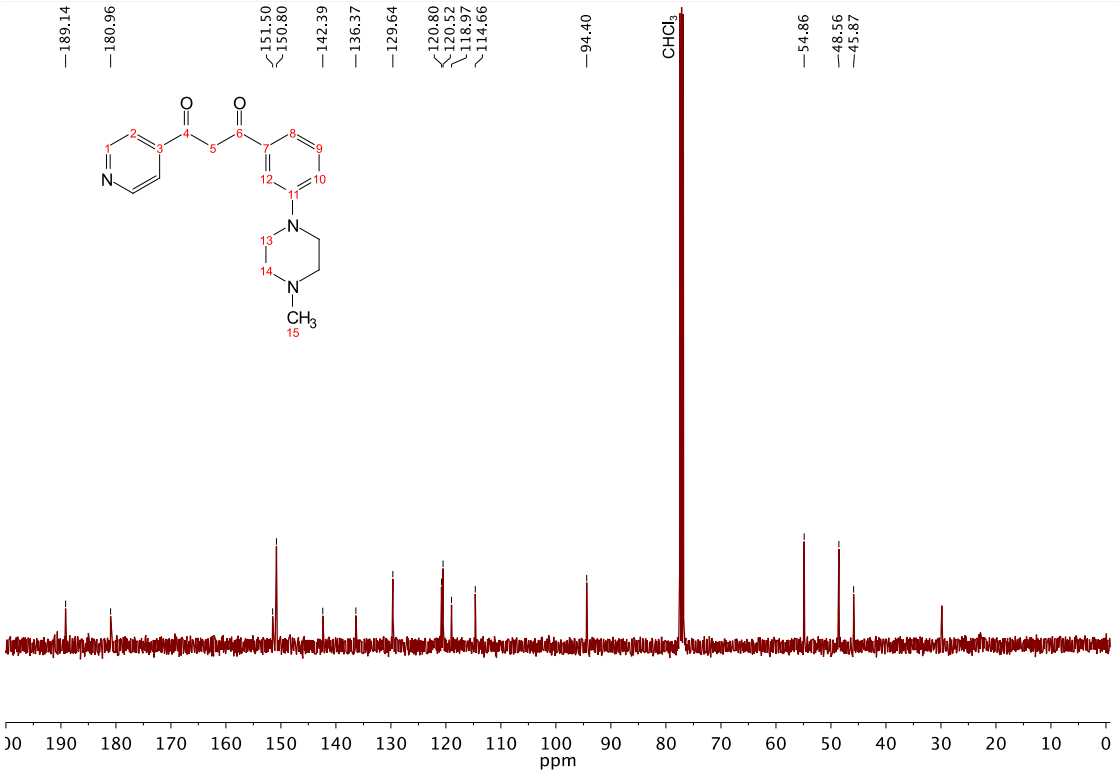

Figure S27. ^{13}C-NMR spectrum of **13** recorded in $CDCl_3$.

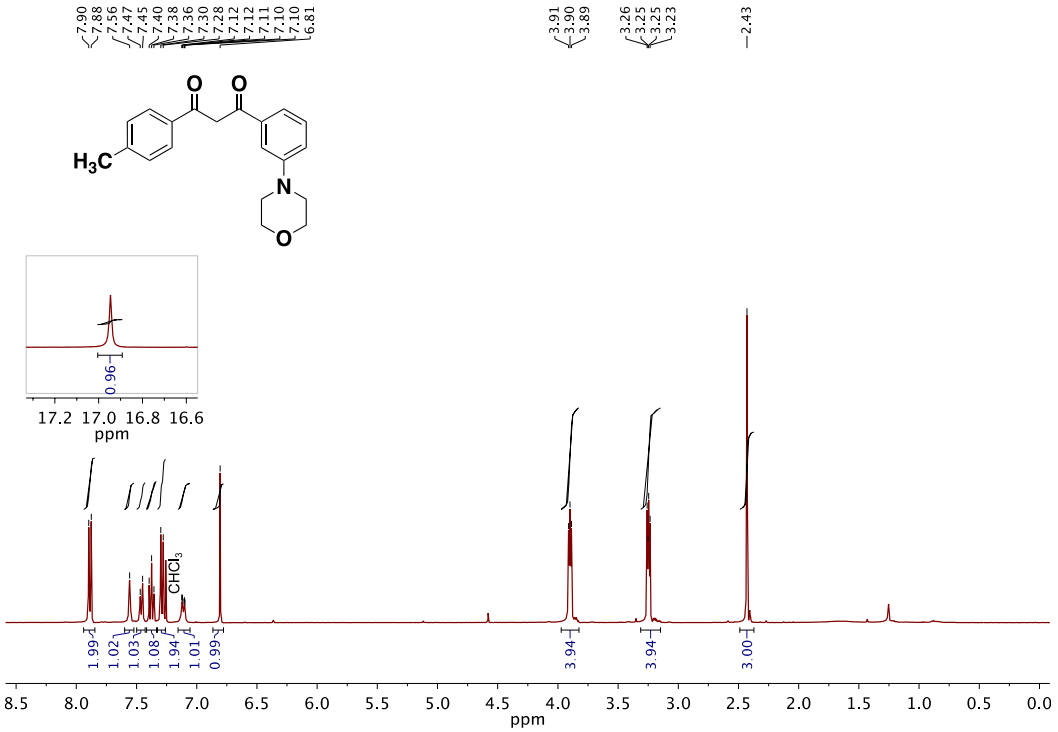

Figure S28. ^{1}H-NMR spectrum of **18** recorded in $CDCl_3$.

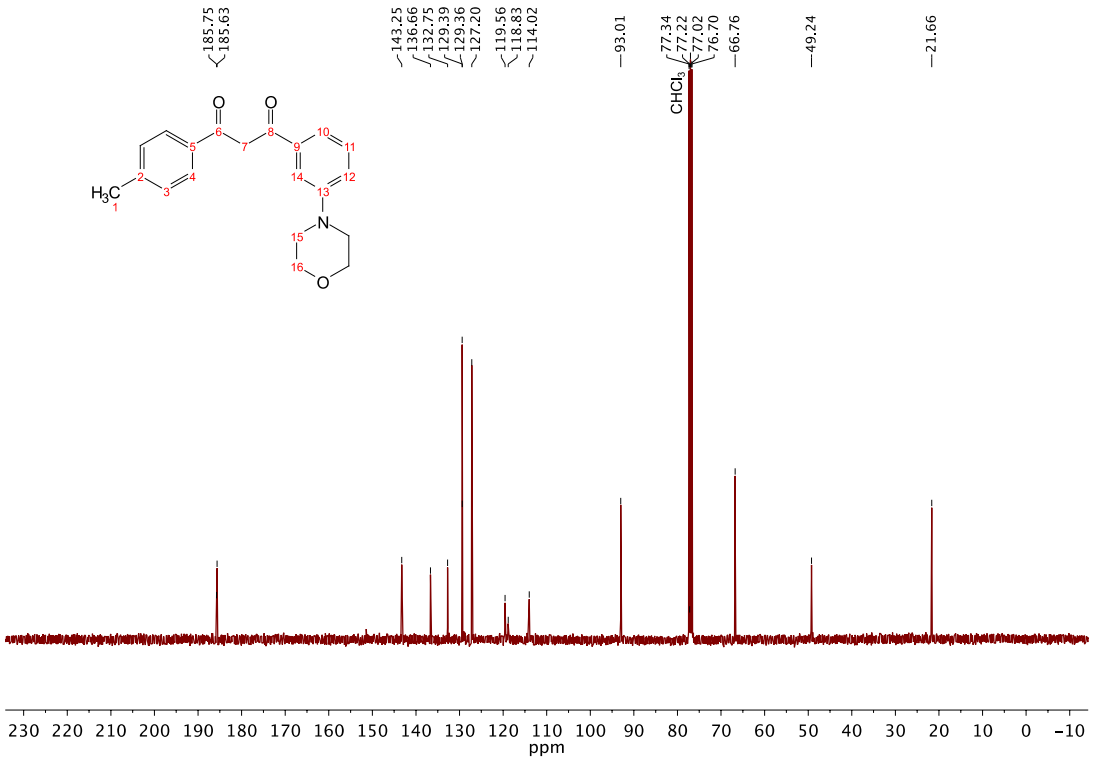

Figure S29. ^{13}C-NMR spectrum of **18** recorded in $CDCl_3$.

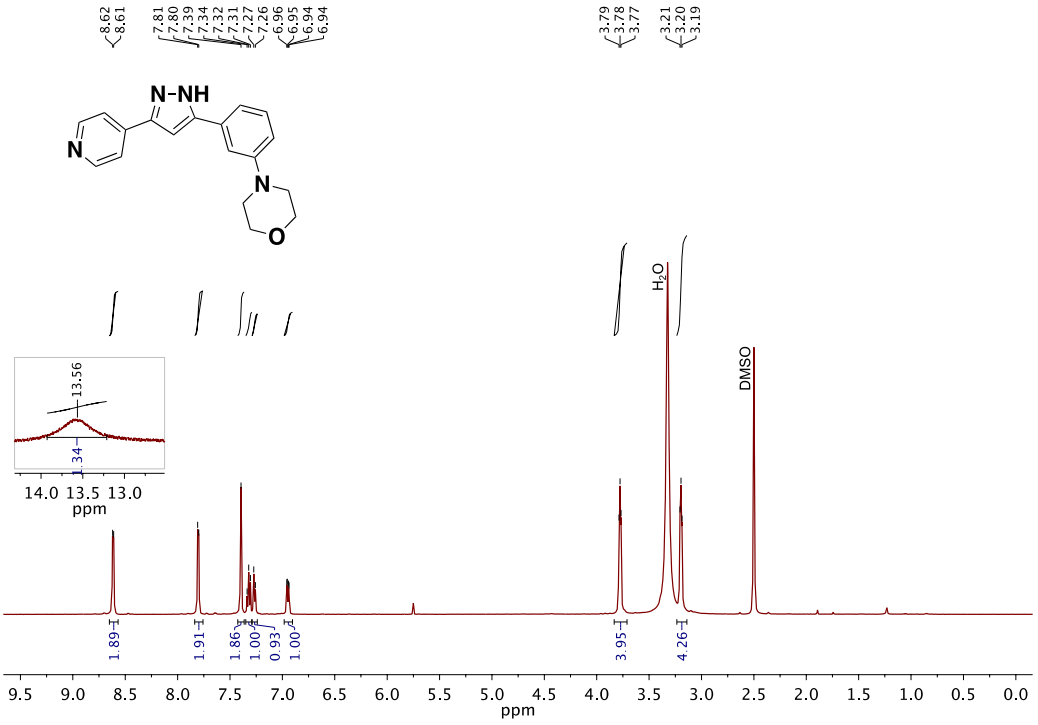

Figure S30. ^{1}H-NMR spectrum of **17** recorded in DMSO-d_6.

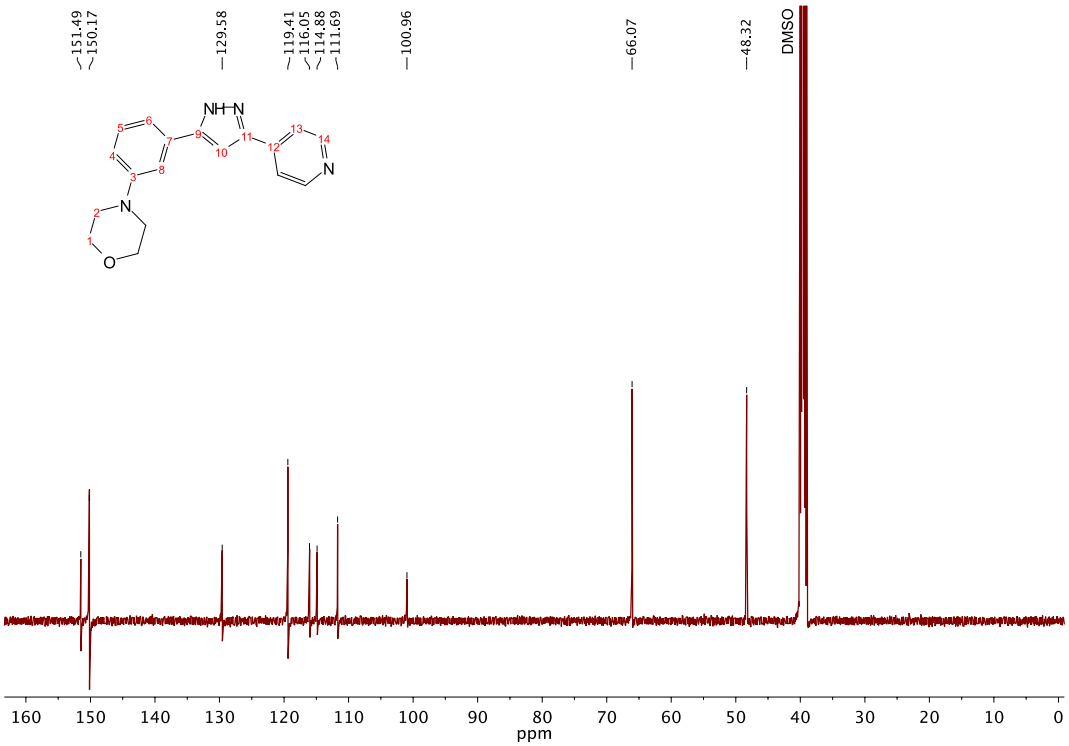

Figure S31. [13]C-NMR spectrum of **17** recorded in DMSO-d_6.

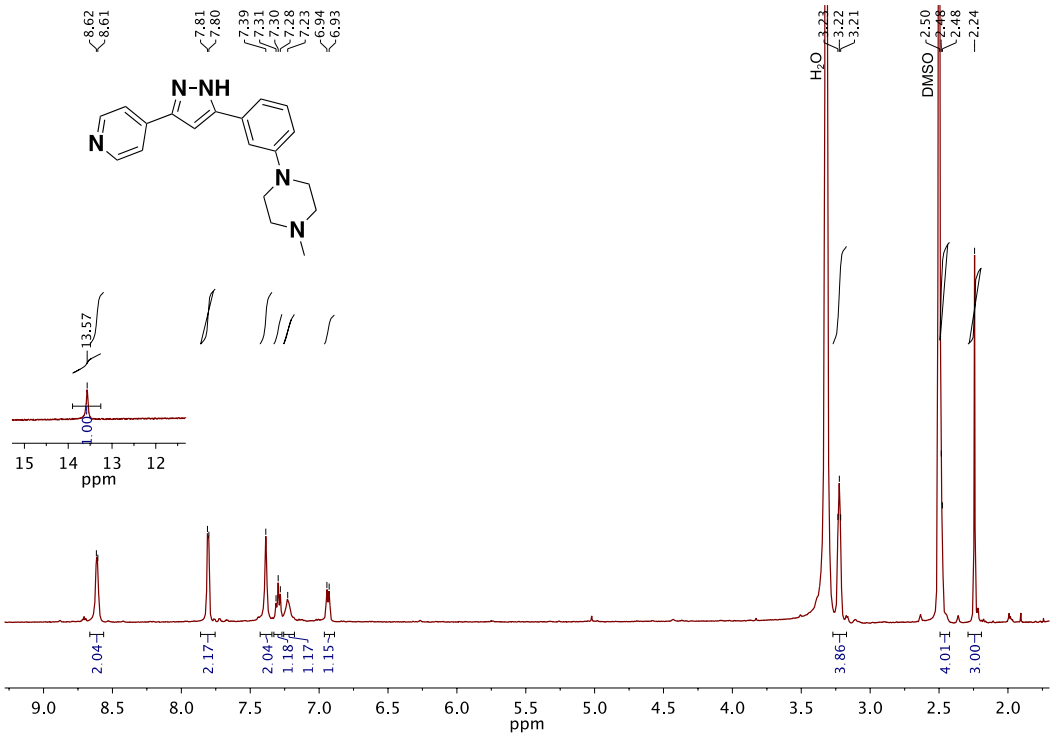

Figure S32. [1]H-NMR spectrum of **15** recorded in DMSO-d_6.

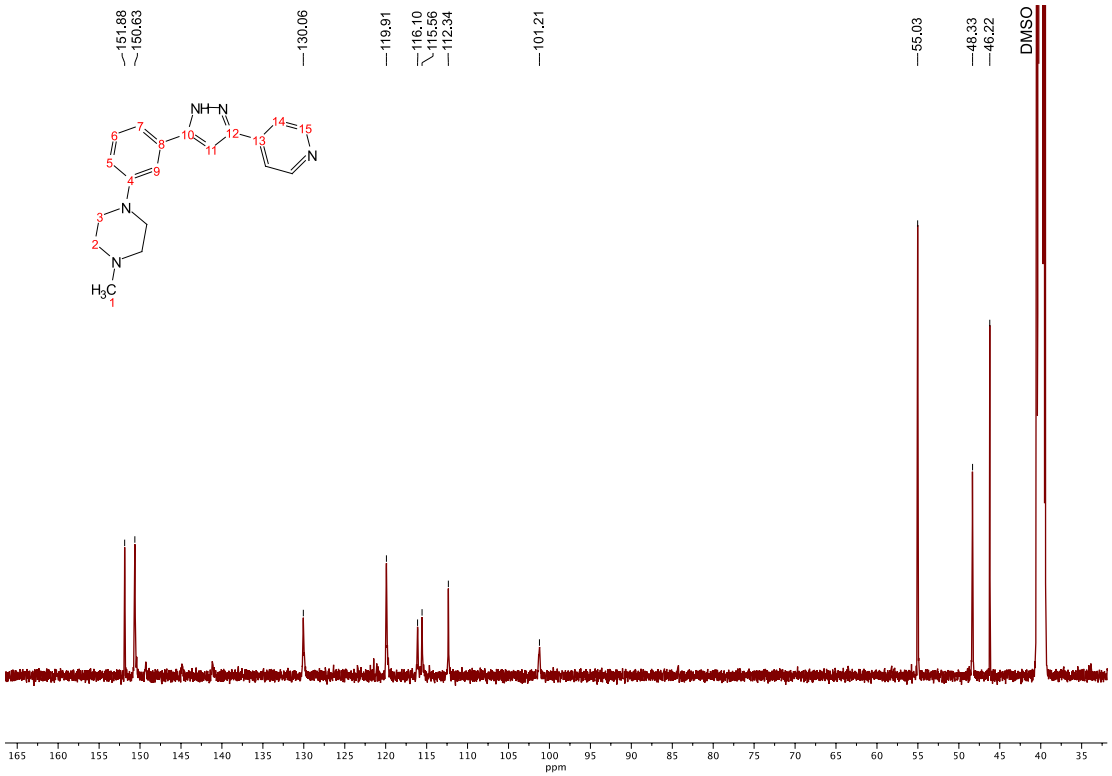

Figure S33. ^{13}C-NMR spectrum of **15** recorded in DMSO-d_6.

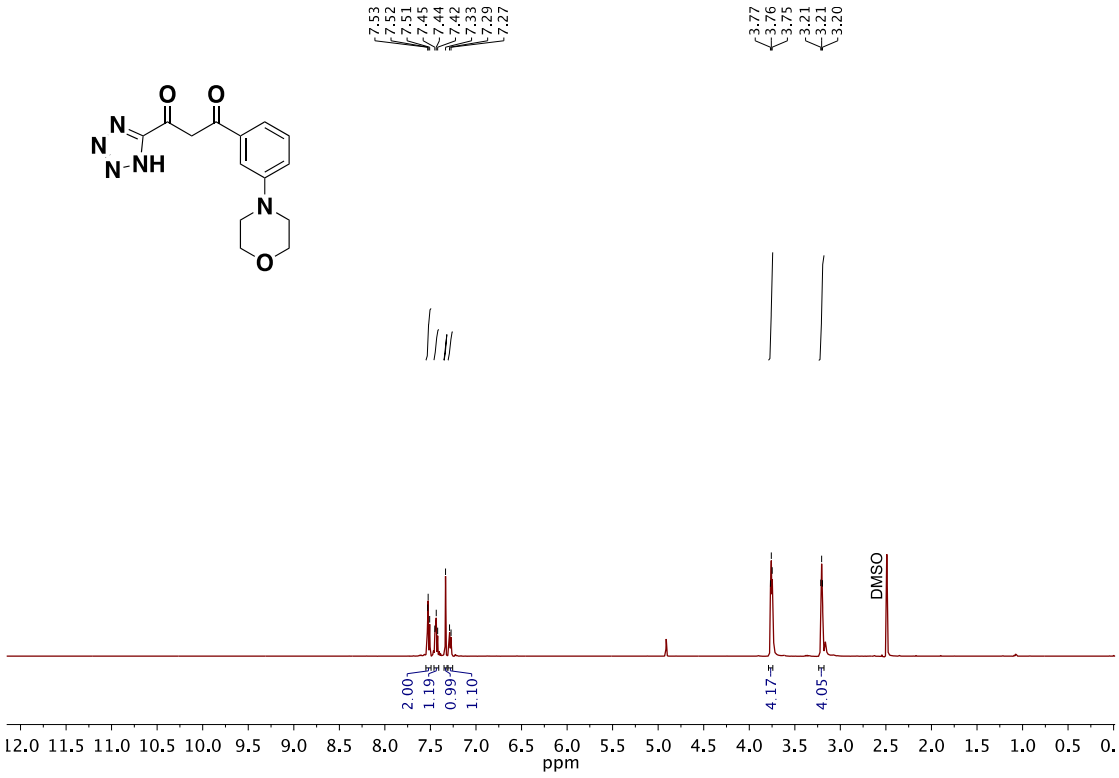

Figure S34. ^{1}H-NMR spectrum of **16** recorded in DMSO-d_6.

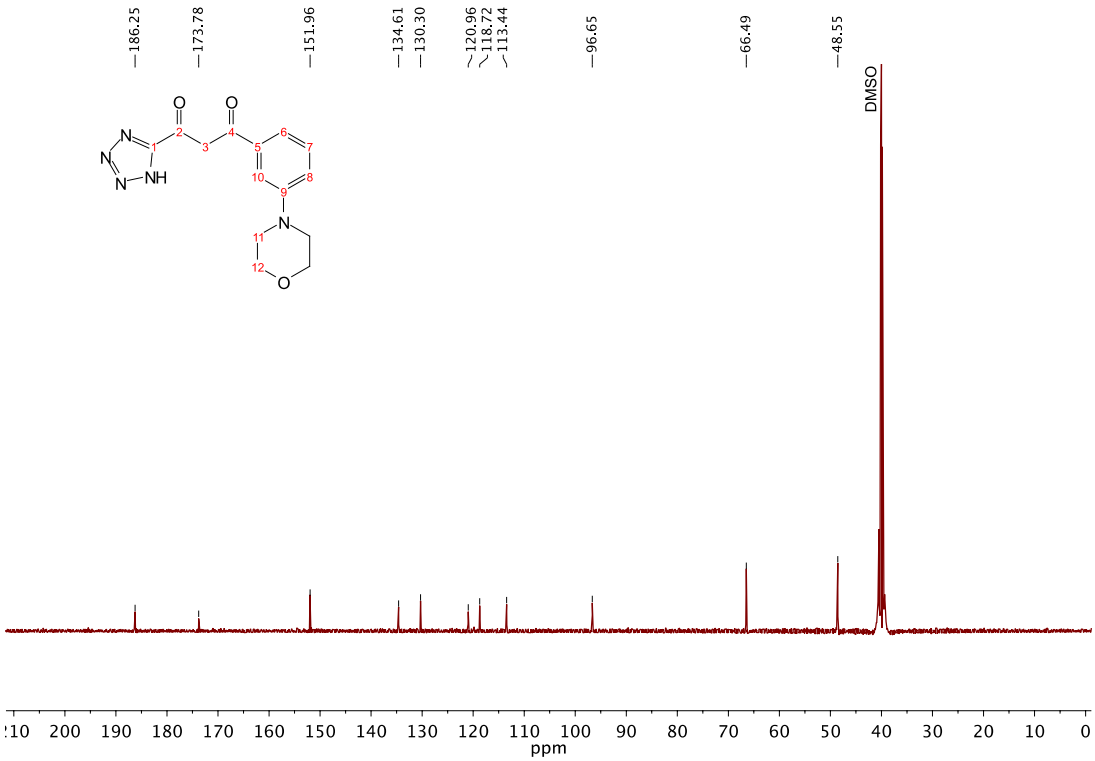

Figure S35. ^{13}C-NMR spectrum of **16** recorded in DMSO-d_6.

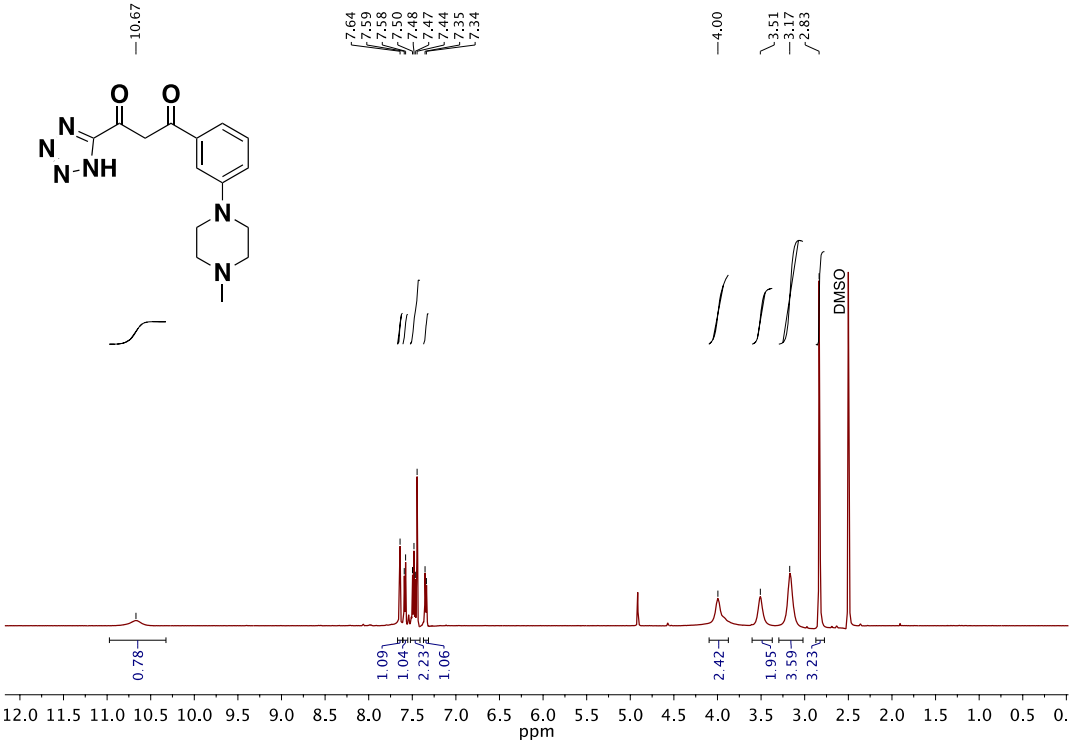

Figure S36. ^{1}H-NMR spectrum of **14** recorded in DMSO-d_6.

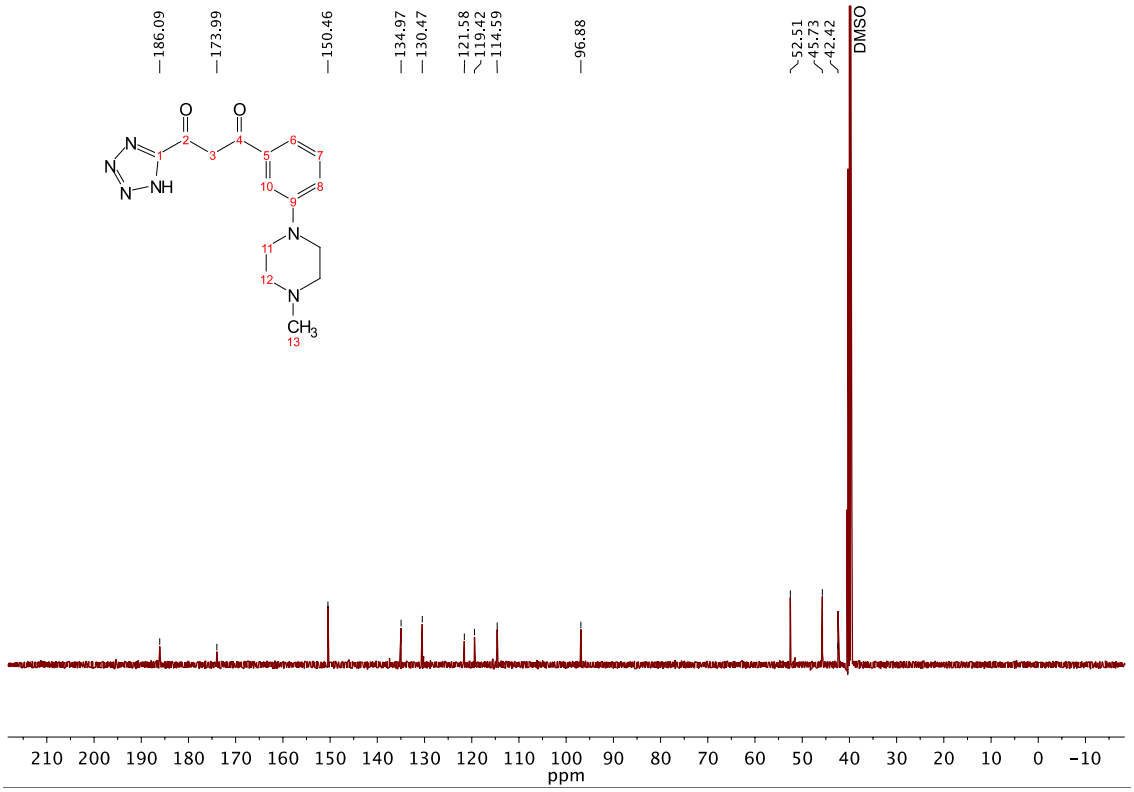

Figure S37. ^{13}C-NMR spectrum of **14** recorded in DMSO-d_6.

3. Supporting tables and figures

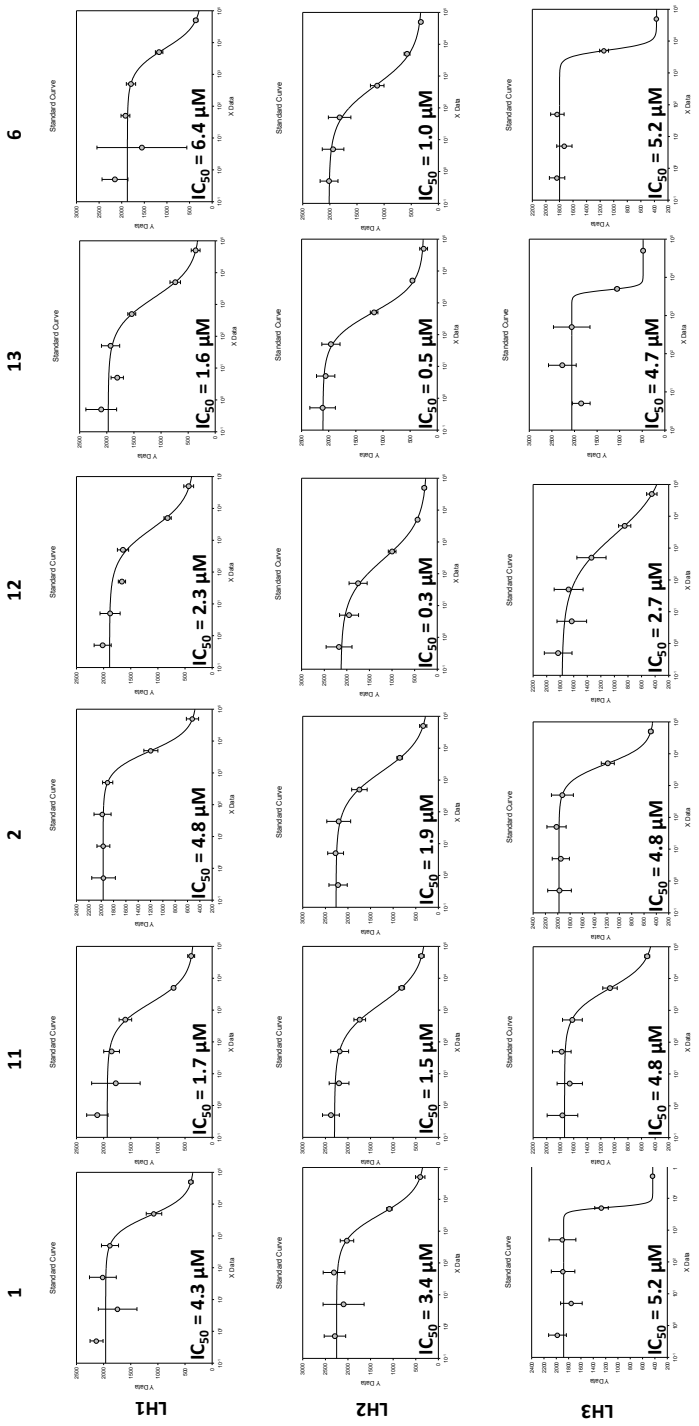

Figure S38. Enzymatic *in vitro* activity assay against all three LH isoforms (LH1-3). Compounds **1**, **2**, **6**, **11**, **12**, and **13** were evaluated.

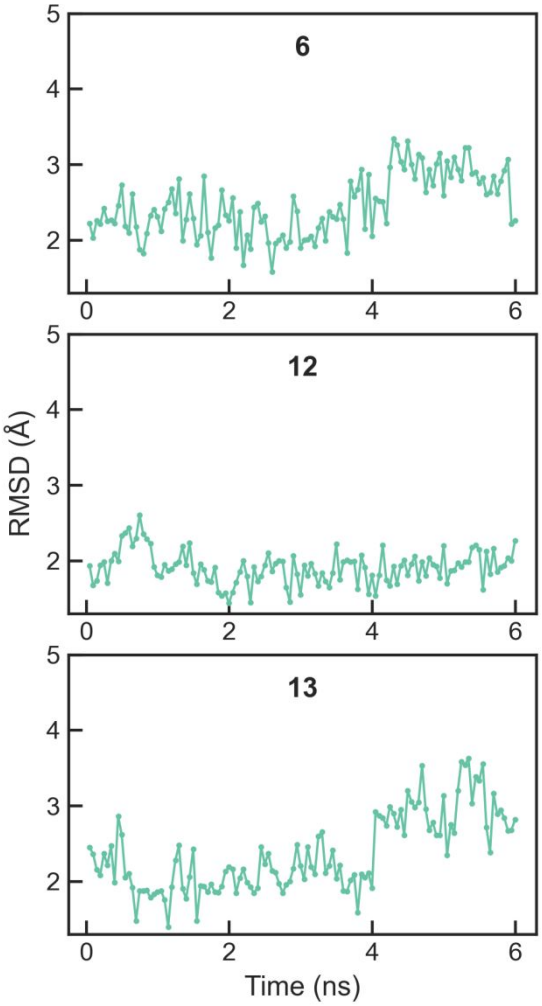

Figures S39. Ligand root mean squared deviation (RMSD) for compounds **6**, **12,** and **13**. The structure was first aligned to the alpha carbons of the initial structure, and then the RMSD was calculated on the ligand atoms without fitting.

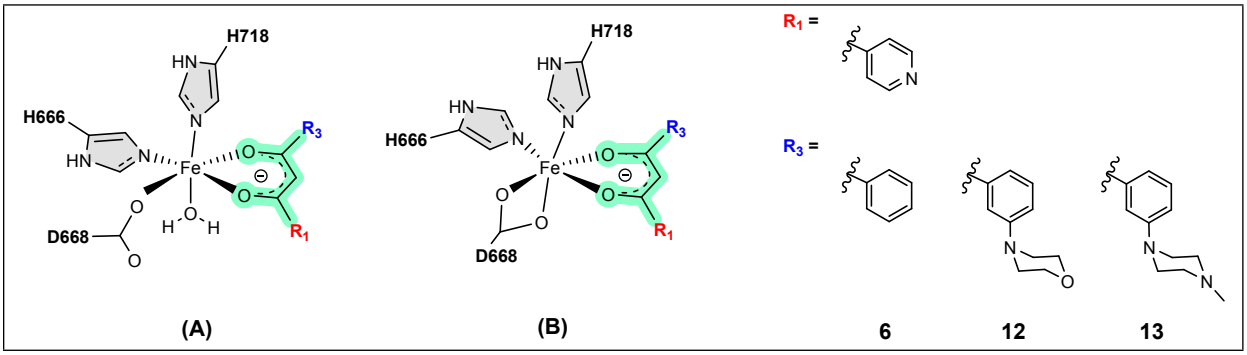

Figure S40. General stereochemistry of the active site in **6** and **12** (A), and **13** (B). The green highlighted residue in (A) and (B) is the enolate part of the ligands.

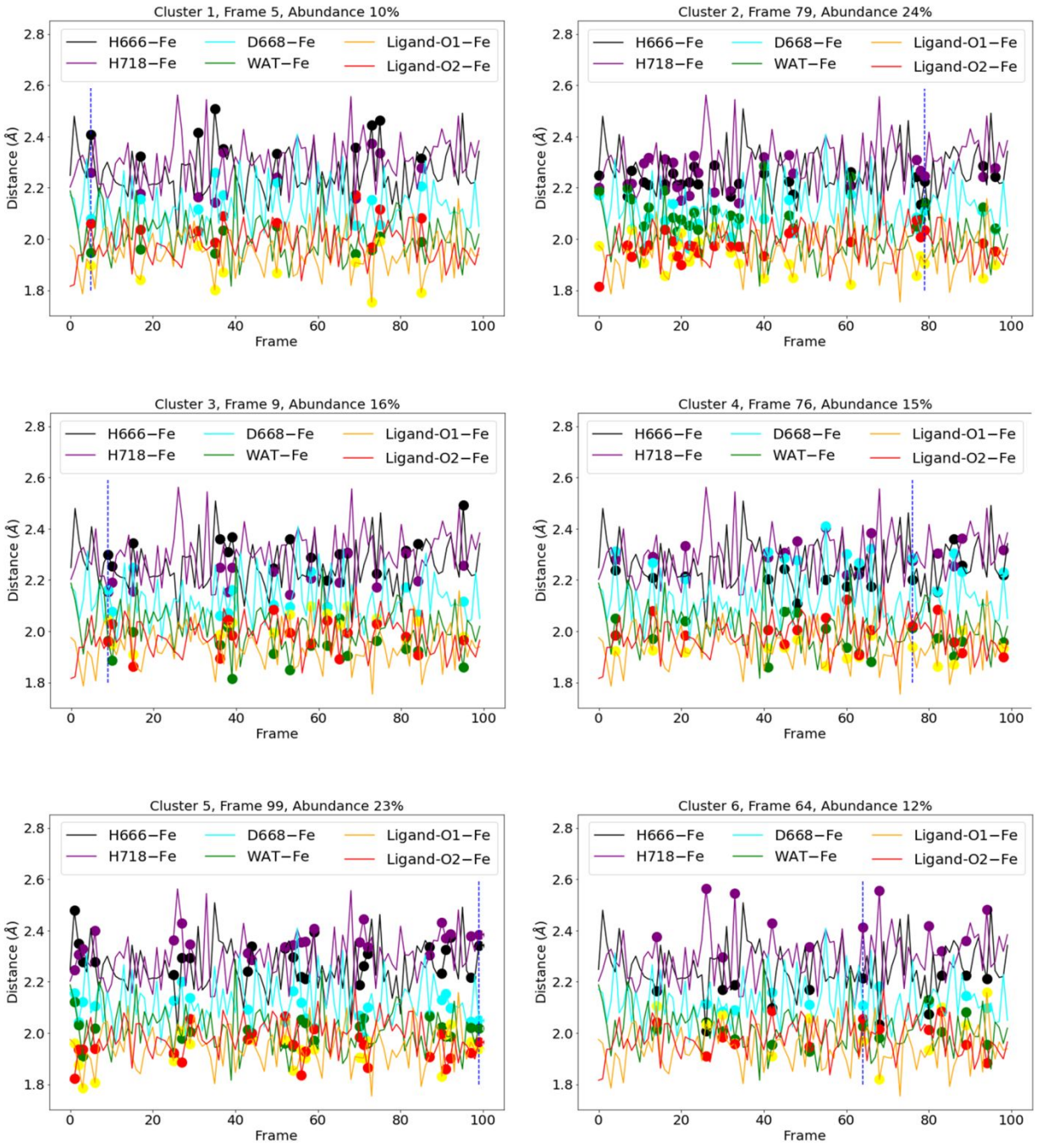

Figure S41. Clusters from the *k*-means analysis for compound **6**. The number of each cluster, related representative/frame, and the abundance percentage are given on top of each graph. The vertical dashed line in each graph shows the closest representative to the centroids of that cluster in all six dimensions. The bold dots show the other frames belong to the cluster.

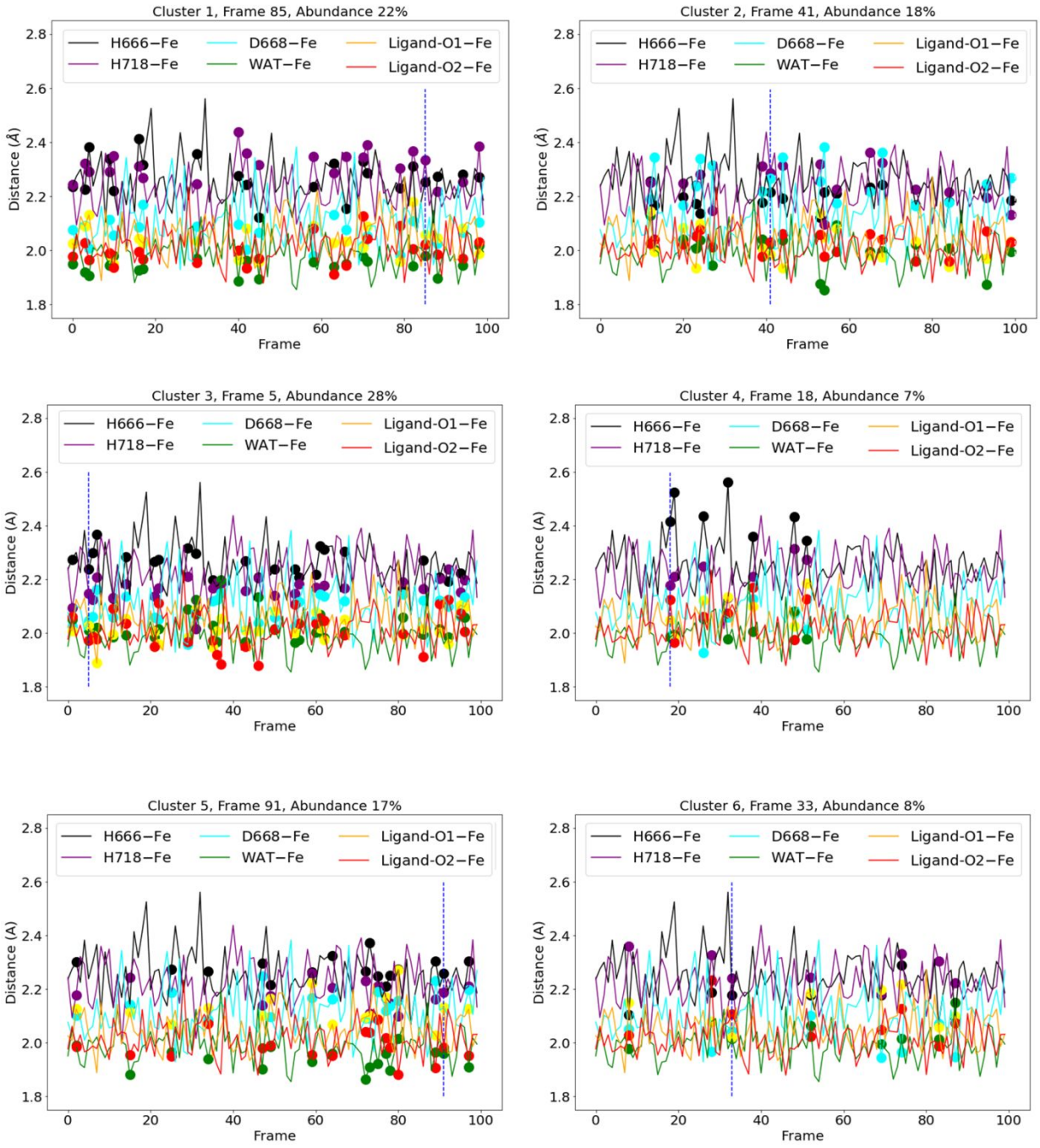

Figure S42. Clusters from the *k*-means analysis for compound **12**. The number of each cluster, related representative/frame, and the abundance percentage are given on top of each graph. The vertical dashed line in each graph shows the closest representative to the centroids of that cluster in all six dimensions. The bold dots show the other frames belong to the cluster.

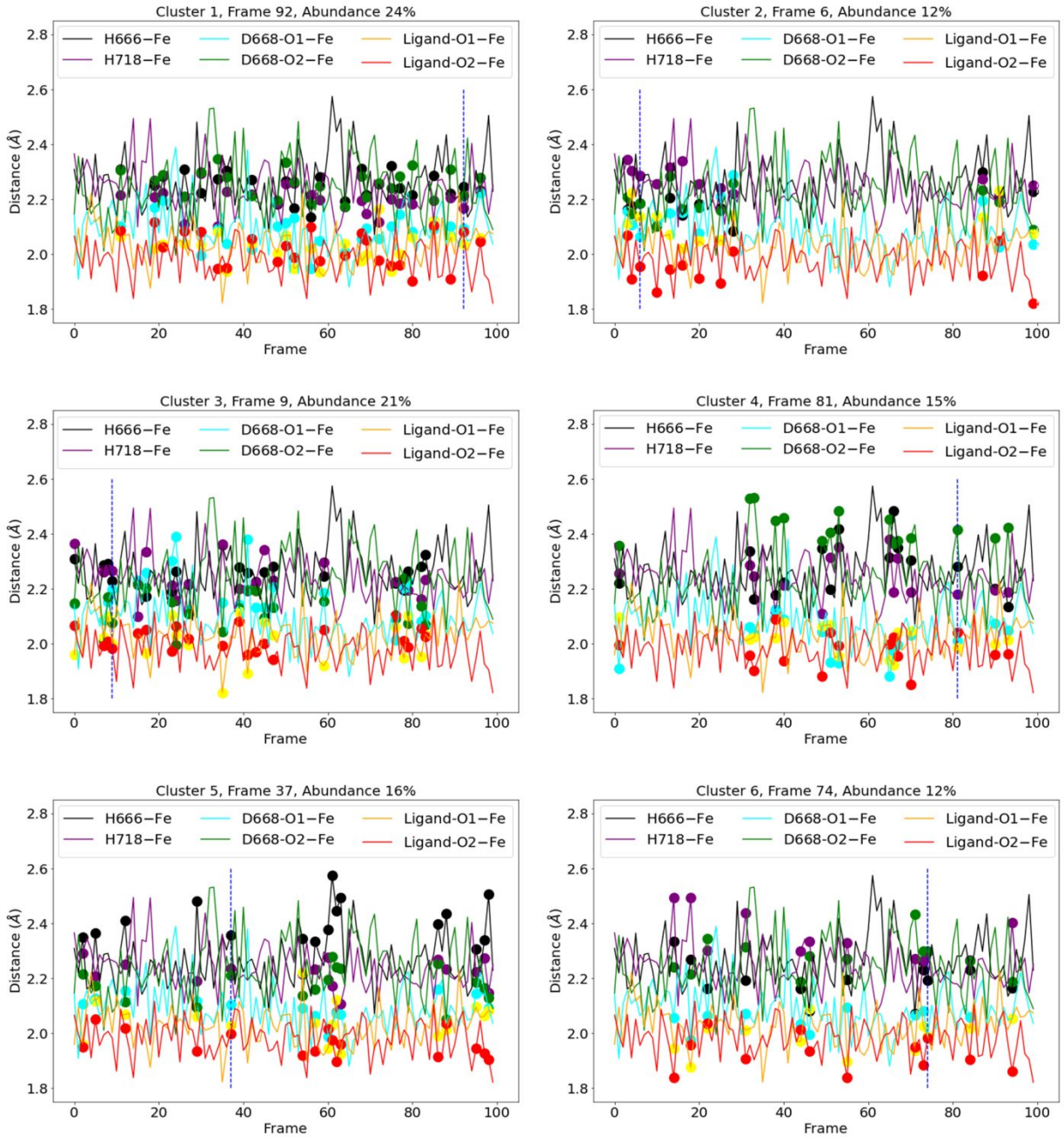

Figure S43. Clusters from the *k*-means analysis for compound **13**. The number of each cluster, related representative/frame, and the abundance percentage are given on top of each graph. The vertical dashed line in each graph shows the closest representative to the centroids of that cluster in all six dimensions. The bold dots show the other frames belong to the cluster.

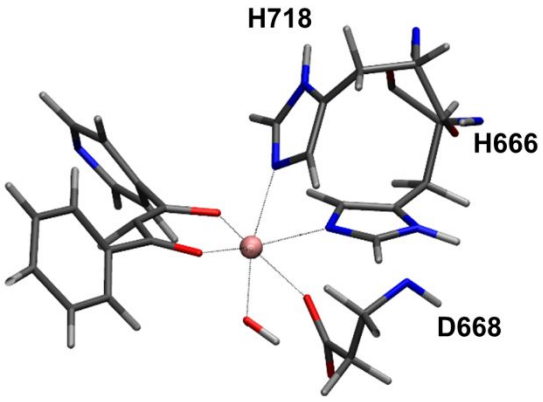

Cluster 1, Frame 5, 10%

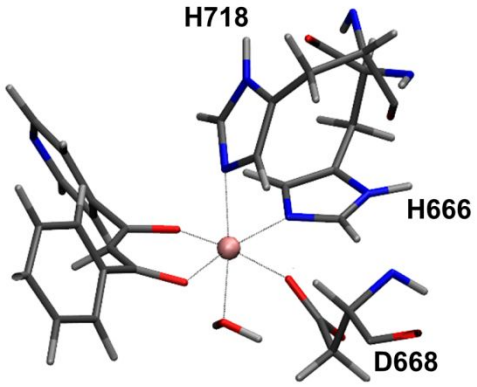

Cluster 2, Frame 79, 24%

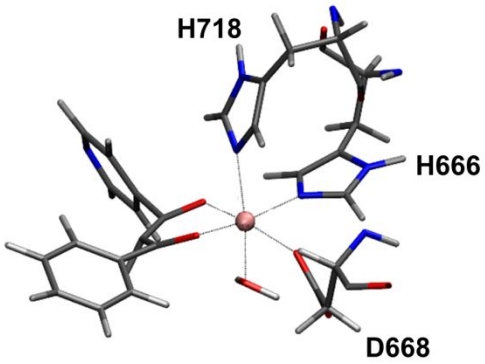

Cluster 3, Frame 9, 16%

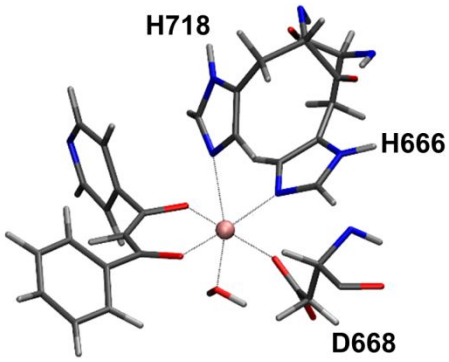

Cluster4, Frame 76, 15%

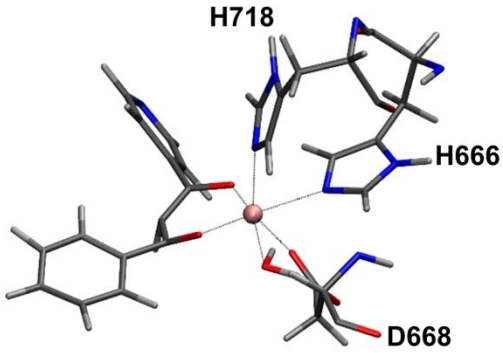

Cluster 5, Frame 99, 23%

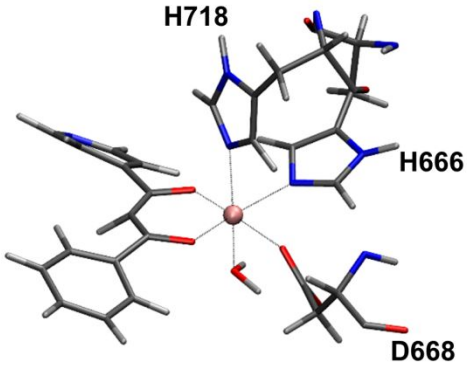

Cluster 6, Frame 64, 12%

Bond	Fe–ASP	Fe–HIS	Fe–Ligand	Fe–WAT
Avg. dist. ± std. dev. (Å)	2.16 ± 0.13	2.27 ± 0.08	1.97 ± 0.07	2.03 ± 0.09

Figure S44. Close-up to show the interactions between Fe(II) and residues of the active site in each representative structure of compound **6**. The distances between the iron and H666, D668, H718, water molecule, and ligand are given in each figure. The MM region is not shown for more clarity.

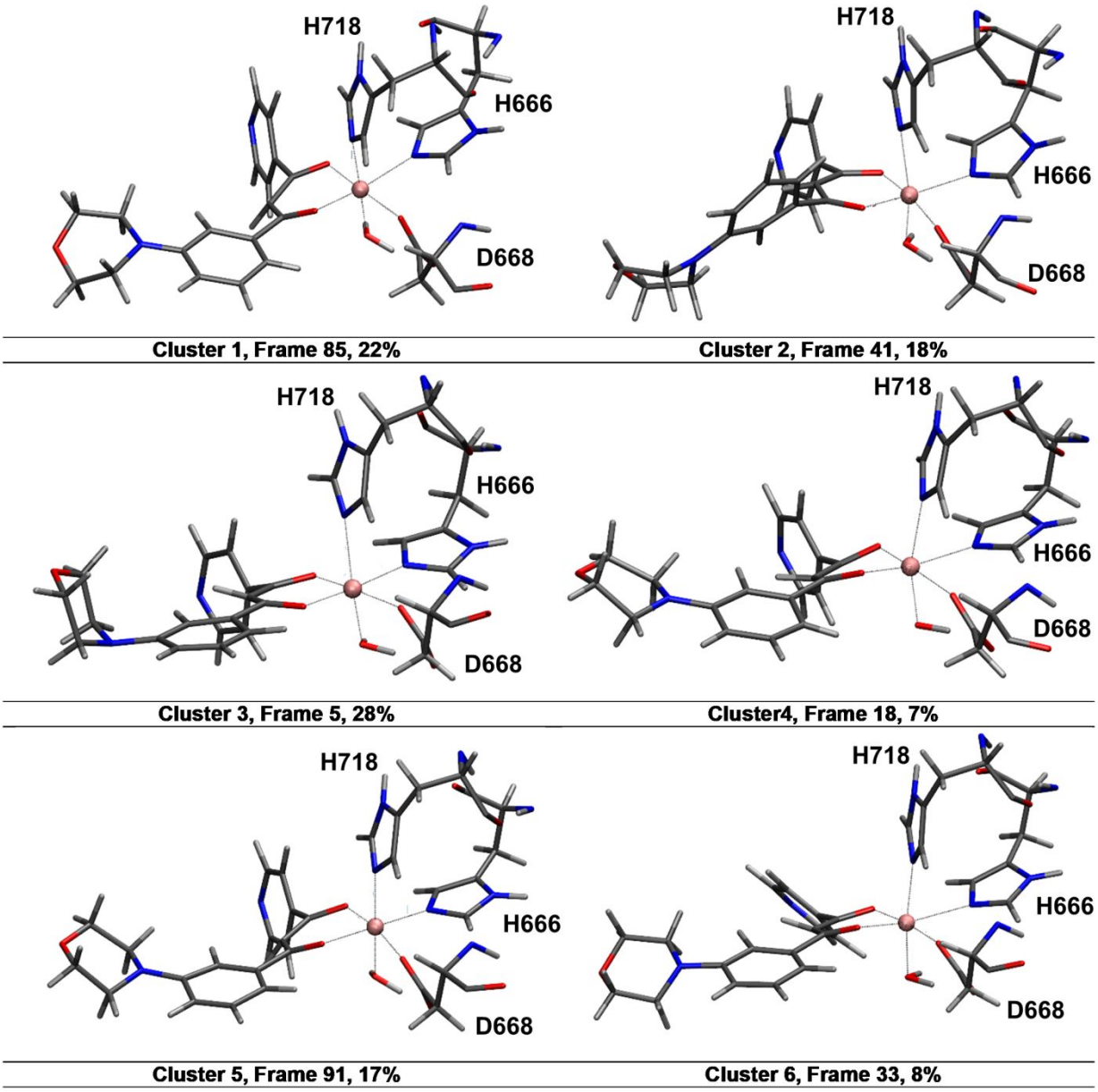

Bond	Fe–ASP	Fe–HIS	Fe–Ligand	Fe–WAT
Avg. dist. ± std. dev. (Å)	2.11 ± 0.06	2.29 ± 0.12	2.01 ± 0.05	1.97 ± 0.05

Figure S45. Close-up to show the interactions between Fe(II) and residues of the active site in each representative structure of compound **12**. The distances between the iron and H666, D668, H718, water molecule, and ligand are given in each figure. The MM region is not shown for more clarity.

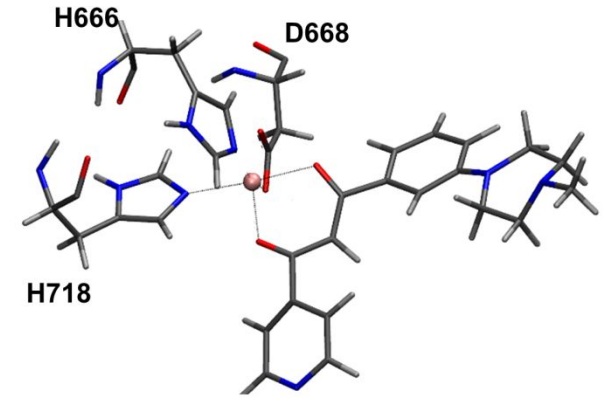

Cluster 1, Frame 92, 24%

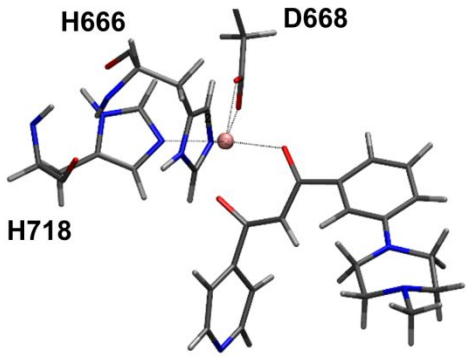

Cluster 2, Frame 6, 12%

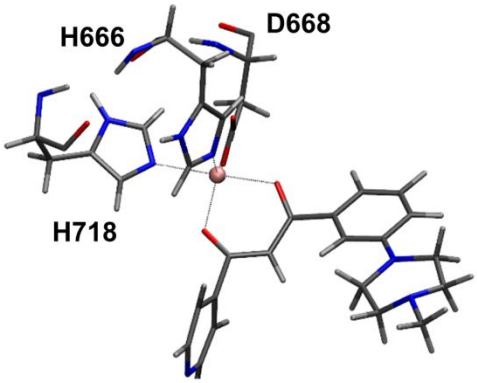

Cluster 3, Frame 9, 21%

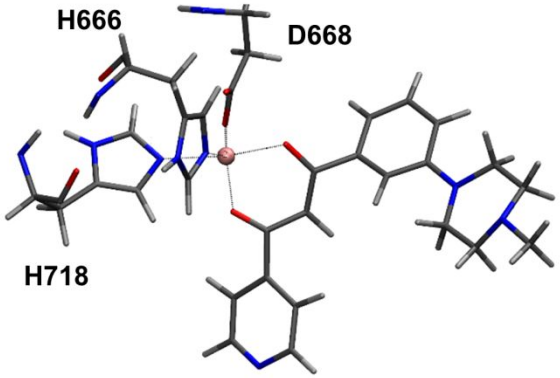

Cluster4, Frame 81, 15%

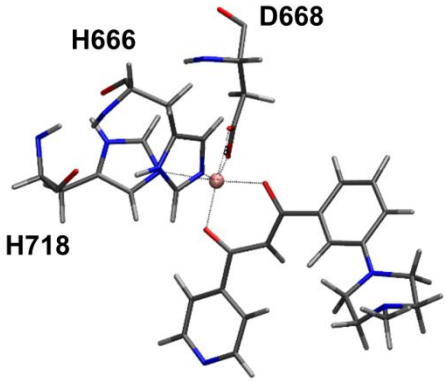

Cluster 5, Frame 37, 16%

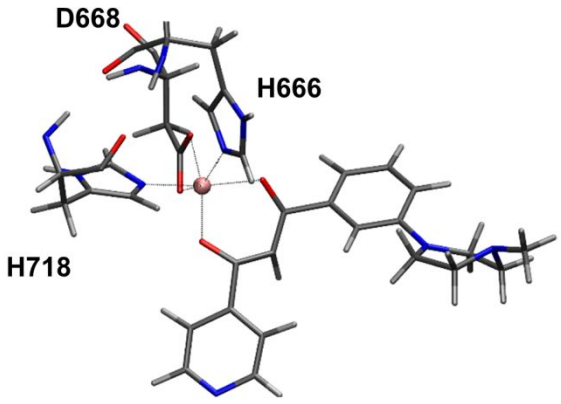

Cluster 6, Frame 74, 12%

Bond	Fe–ASP	Fe–HIS	Fe–Ligand
Avg. dist. ± std. dev. (Å)	2.12 ± 0.09	2.27 ± 0.05	2.07 ± 0.19

Figure S46. Close-up to show the interactions between Fe(II) and residues of the active site in each representative structure of compound **13**. The distances between the iron and H666, D668, H718, and ligand are given in each figure. The MM region is not shown for more clarity.

Table S1. The results of the *k*-means clustering analysis for each system include the number of clusters, position of the centroid in the trajectory, percentage, and average distance. The last column lists the calculated relative QM/MM optimization energies (eV) for each system's representative frames at ωB97X-D/6–31G(d,p) level of theory with AMOEBABIO18 polarizable force field.

Compound	No. cluster	Position (ns)	Position (frame)	Percentage (%)	Relative optimization Energy (eV)
6	1	0.25	5	10	84
	2	3.95	79	24	90
	3	0.45	9	16	43
	4	3.80	76	15	39
	5	4.95	99	23	0
	6	3.20	64	12	87
12	1	4.25	85	22	140
	2	2.05	41	18	10
	3	0.25	5	28	0
	4	0.90	18	7	249
	5	4.55	91	17	125
	6	1.62	33	8	239
13	1	4.60	92*	24	140
	2	0.30	6	12	179
	3	0.45	9	21	236
	4	4.05	81	15	122
	5	1.85	37	16	171
	6	3.70	74*	12	0

*In the case of compound **13**, frame 74, with a cluster percentage of 12% is the most stable structure *but* with the lowest relative energy, while frame 92 has the highest cluster percentage of 24% but with higher energy of 140 eV. In this case, IE_{QMMM} (see Table S2) was calculated for both frames to consider both the representative with the lowest optimization energy and the representative with the highest population.

Table S2. Calculated values of the QM and MM components of the interaction energies (IE) for all three systems at ωB97X-D/6–31G(d,p) level of theory with AMOEBABIO18 polarizable force field. All the values are in Hartree, otherwise stated.

QM/MM components	Compound			
	6	**12**	**13 (frame 74)***	**13 (frame 92)***
$QM_{Active\ site+Ligand}$	–38840.6206	–38303.8954	–38410.8483	–36907.7499
$MM_{LH2+Ligand}$	–202.3891	–200.8681	–195.7376	–198.0642
$QM_{Active\ site}$	–37809.3013	–37253.1502	–37360.1305	–36163.0193
QM_{Ligand}	–1031.0044	–1050.4306	–1050.4305	–744.4751
MM_{LH2}	–202.2898	–200.8380	–195.7060	–198.0008
IE_{QM}	–0.3149	–0.3146	–0.2873	–0.2555
IE_{MM}	–0.0993	–0.0301	−0.0317	–0.0634
IE_{QMMM}	–0.4142	–0.3447	−0.3190	–0.3189
IE_{QM} *(kcal mol^{-1})***	–160.3	–197.6	–197.4	–180.3
IE_{MM} *(kcal mol^{-1})***	–39.8	–62.3	–18.9	–19.9
$IE_{QM/MM}$ *(kcal mol^{-1})****	–200.1	–259.9	–216.3	–200.2

* Calculated values for two representatives of compound **13** (frames 74 and 92) indicate that frame 74, which corresponds to the lowest optimization energy (see Table S1), also has the lowest $IE_{QM/MM}$. The ~16 kcal mol^{-1} calculated energy difference between frames 74 and 92 is due to a stronger interaction between **13** and the active site in frame 74, as opposed to a stabilization due to the MM subsystem. Based on these results, frame 74 was used for further study and calculations in the main text.

** Interactions due to the QM region (IE_{QM}) and the MM region (IE_{MM}).

*** $IE_{QM/MM} = [QM_{active\ site\ +\ ligand} - (QM_{active\ site} + QM_{ligand})] + [MM_{LH2\ +\ ligand} - MM_{LH2}]$

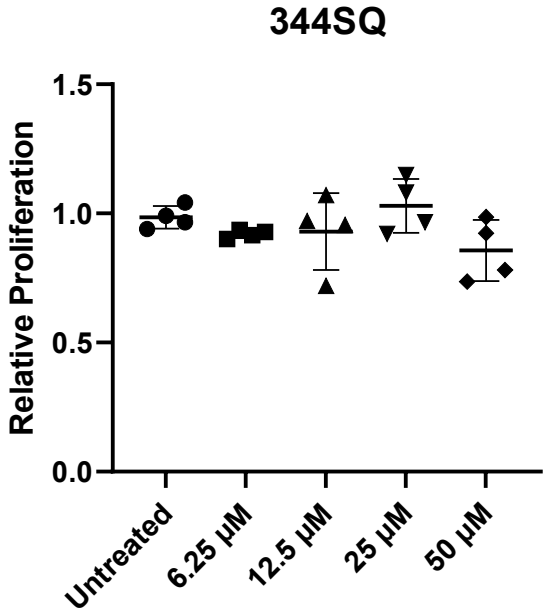

Figure S47. The cell proliferation assay. Graphs showing the cell proliferation for 344SQ with varying concentrations of **13**.

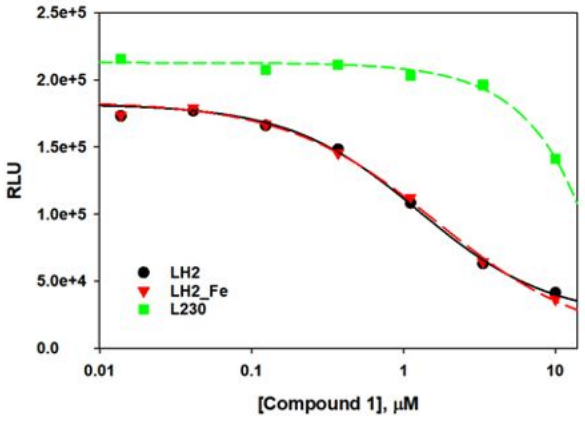

Condition	10 µM Fe^{2+}	100 µM Fe^{2+}
IC_{50}, µM	1.26	1.65
H coefficient	1.01	0.87
r^2	0.994	0.995

Figure S48. Activity profile of compound **1** in the presence of 10 µM Fe^{2+} (LH2, black circle) and a 10-fold excess of Fe^{2+} (LH2_100Fe, red inverted triangle). The change in the relative luminescence units (RLU) (and the binding parameters) was comparable between LH2 and LH_100Fe, supporting that the compound's activity is not due to Fe^{2+} chelation. Additionally, the activity of a viral ortholog of LH2, L230 (green square), decreases only slightly at the highest concentration of compound **1**, indicating that compound **1** is selective to LH2 and is not interfering with assay components.

4. References

1. Yamauchi, M.; Barker, T. H.; Gibbons, D. L.; Kurie, J. M., The fibrotic tumor stroma. *J Clin Invest* **2018,** *128* (1), 16-25.
2. Guo, H. F.; Cho, E. J.; Devkota, A. K.; Chen, Y.; Russell, W.; Phillips, G. N., Jr.; Yamauchi, M.; Dalby, K. N.; Kurie, J. M., A scalable lysyl hydroxylase 2 expression system and luciferase-based enzymatic activity assay. *Arch Biochem Biophys* **2017,** *618*, 45-51.
3. Guo, H. F.; Tsai, C. L.; Terajima, M.; Tan, X.; Banerjee, P.; Miller, M. D.; Liu, X.; Yu, J.; Byemerwa, J.; Alvarado, S.; Kaoud, T. S.; Dalby, K. N.; Bota-Rabassedas, N.; Chen, Y.; Yamauchi, M.; Tainer, J. A.; Phillips, G. N., Jr.; Kurie, J. M., Pro-metastatic collagen lysyl hydroxylase dimer assemblies stabilized by Fe(2+)-binding. *Nat Commun* **2018,** *9* (1), 512.
4. Guo, H. F.; Bota-Rabassedas, N.; Terajima, M.; Leticia Rodriguez, B.; Gibbons, D. L.; Chen, Y.; Banerjee, P.; Tsai, C. L.; Tan, X.; Liu, X.; Yu, J.; Tokmina-Roszyk, M.; Stawikowska, R.; Fields, G. B.; Miller, M. D.; Wang, X.; Lee, J.; Dalby, K. N.; Creighton, C. J.; Phillips, G. N., Jr.; Tainer, J. A.; Yamauchi, M.; Kurie, J. M., A collagen glucosyltransferase drives lung adenocarcinoma progression in mice. *Commun Biol* **2021,** *4* (1), 482.
5. Maghsoud, Y.; Vázquez-Montelongo, E. A.; Yang, X.; Liu, C.; Jing, Z.; Lee, J.; Harger, M.; Smith, A. K.; Espinoza, M.; Guo, H.-F.; Kurie, J. M.; Dalby, K. N.; Ren, P.; Cisneros, G.A., Computational Investigation of a Series of Small Molecules as Potential Compounds for Lysyl hydroxylase-2 (LH2) Inhibition. *J. Chem. Inf. Model.* **2023**, *63*(3) 986-1001.
6. Waterhouse, A.; Bertoni, M.; Bienert, S.; Studer, G.; Tauriello, G.; Gumienny, R.; Heer, F. T.; de Beer, T. A. P.; Rempfer, C.; Bordoli, L., SWISS-MODEL: homology modelling of protein structures and complexes. *Nucleic acids research* **2018,** *46* (W1), W296-W303.
7. Harger, M.; Li, D.; Wang, Z.; Dalby, K.; Lagardère, L.; Piquemal, J.-P.; Ponder, J.; Ren, P., Tinker-OpenMM: Absolute and relative alchemical free energies using AMOEBA on GPUs. *Journal of Computational Chemistry* **2017,** *38* (23), 2047-2055.

8. Likas, A.; Vlassis, N.; Verbeek, J. J., The global k-means clustering algorithm. *Pattern recognition* **2003,** *36* (2), 451-461.
9. Kratz, E. G.; Walker, A. R.; Lagardère, L.; Lipparini, F.; Piquemal, J. P.; Andrés Cisneros, G., LICHEM: A QM/MM program for simulations with multipolar and polarizable force fields. *Journal of computational chemistry* **2016,** *37* (11), 1019-1029.
10. Gökcan, H.; Vázquez-Montelongo, E. A.; Cisneros, G. A., LICHEM 1.1: recent improvements and new capabilities. *Journal of chemical theory and computation* **2019,** *15* (5), 3056-3065.
11. Frisch, M. J.; Trucks, G. W.; Schlegel, H. B.; Scuseria, G. E.; Robb, M. A.; Cheeseman, J. R.; Scalmani, G.; Barone, V.; Petersson, G. A.; Nakatsuji, H.; Li, X.; Caricato, M.; Marenich, A. V.; Bloino, J.; Janesko, B. G.; Gomperts, R.; Mennucci, B.; Hratchian, H. P.; Ortiz, J. V.; Izmaylov, A. F.; Sonnenberg, J. L.; Williams; Ding, F.; Lipparini, F.; Egidi, F.; Goings, J.; Peng, B.; Petrone, A.; Henderson, T.; Ranasinghe, D.; Zakrzewski, V. G.; Gao, J.; Rega, N.; Zheng, G.; Liang, W.; Hada, M.; Ehara, M.; Toyota, K.; Fukuda, R.; Hasegawa, J.; Ishida, M.; Nakajima, T.; Honda, Y.; Kitao, O.; Nakai, H.; Vreven, T.; Throssell, K.; Montgomery Jr., J. A.; Peralta, J. E.; Ogliaro, F.; Bearpark, M. J.; Heyd, J. J.; Brothers, E. N.; Kudin, K. N.; Staroverov, V. N.; Keith, T. A.; Kobayashi, R.; Normand, J.; Raghavachari, K.; Rendell, A. P.; Burant, J. C.; Iyengar, S. S.; Tomasi, J.; Cossi, M.; Millam, J. M.; Klene, M.; Adamo, C.; Cammi, R.; Ochterski, J. W.; Martin, R. L.; Morokuma, K.; Farkas, O.; Foresman, J. B.; Fox, D. J. *Gaussian 16 Rev. C.01*, Wallingford, CT, 2016.
12. Rackers, J. A.; Wang, Z.; Lu, C.; Laury, M. L.; Lagardère, L.; Schnieders, M. J.; Piquemal, J.-P.; Ren, P.; Ponder, J. W., Tinker 8: software tools for molecular design. *Journal of chemical theory and computation* **2018,** *14* (10), 5273-5289.
13. Chai, J.-D.; Head-Gordon, M., Long-range corrected hybrid density functionals with damped atom–atom dispersion corrections. *Physical Chemistry Chemical Physics* **2008,** *10* (44), 6615-6620.
14. Chai, J.-D.; Head-Gordon, M., Systematic optimization of long-range corrected hybrid density functionals. *The Journal of chemical physics* **2008,** *128* (8), 084106.

15. Zhang, C.; Lu, C.; Jing, Z.; Wu, C.; Piquemal, J.-P.; Ponder, J. W.; Ren, P., AMOEBA polarizable atomic multipole force field for nucleic acids. *Journal of chemical theory and computation* **2018,** *14* (4), 2084-2108.
16. Lu, T.; Chen, F., Multiwfn: a multifunctional wavefunction analyzer. *Journal of computational chemistry* **2012,** *33* (5), 580-592.
17. Johnson, E. R.; Keinan, S.; Mori-Sánchez, P.; Contreras-García, J.; Cohen, A. J.; Yang, W., Revealing noncovalent interactions. *Journal of the American Chemical Society* **2010,** *132* (18), 6498-6506.
18. Humphrey, W.; Dalke, A.; Schulten, K., VMD: visual molecular dynamics. *Journal of molecular graphics* **1996,** *14* (1), 33-38.
19. Jurcik, A.; Bednar, D.; Byska, J.; Marques, S. M.; Furmanova, K.; Daniel, L.; Kokkonen, P.; Brezovsky, J.; Strnad, O.; Stourac, J., CAVER Analyst 2.0: analysis and visualization of channels and tunnels in protein structures and molecular dynamics trajectories. *Bioinformatics* **2018,** *34* (20), 3586-3588.
20. Petřek, M.; Otyepka, M.; Banáš, P.; Košinová, P.; Koča, J.; Damborský, J., CAVER: a new tool to explore routes from protein clefts, pockets, and cavities. *BMC bioinformatics* **2006,** *7* (1), 1-9.